Macromolecules

pubs.acs.org/Macromolecules Article

Tunable Electric Double-Layer Capacitor Performance through Engineered Charge Patterns in Polyelectrolytes

Yan Sui, Tingting Yin, Zixiao Yang, Yichun Zhao, Xiaoyu Kong, Dongluo Wu, Jiajia Zhou, Xiupeng Chen, and Xian Kong*

Cite This: *Macromolecules* 2025, 58, 6883−6896 Read Online

ACCESS | Metrics & More | Article Recommendations | Supporting Information

ABSTRACT: Understanding how charge fraction and sequence in polyelectrolytes (PEs) affect electric double-layer capacitors (EDLCs) is crucial for optimizing energy storage devices. We employed antisymmetric PEs composed of polycations and polyanions with identical charge patterns, eliminating counterion effects and focusing on intrinsic PE−electrode interactions. Our simulations revealed that increasing the charge fraction enhances differential capacitance due to more charged species facilitating efficient charge storage. Block-patterned PEs, where charged beads are grouped along the polymer chain, exhibited higher integral capacitance than regular-patterned PEs and simple electrolytes but resulted in slower charging rates due to substantial conformational adjustments during adsorption. Both types of PEs promoted enhanced overscreening, increasing the charge accumulation near the electrode surface. These findings highlight the significant impact of the charge fraction and sequence on the EDLC performance. Careful selection of PE charge patterns can thus tailor energy storage capacities and charging rates to meet specific application needs.

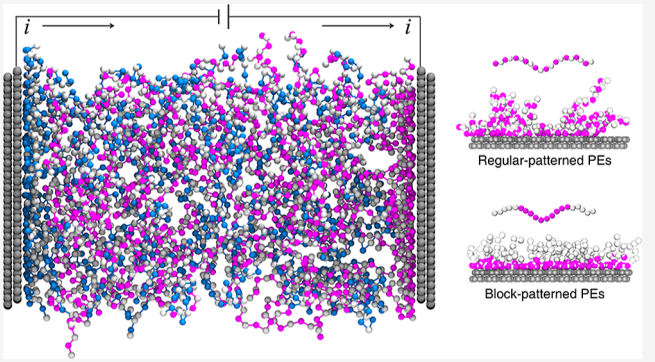

INTRODUCTION

Electrochemical energy storage devices are essential for harnessing clean and renewable energy. Among them, supercapacitors are notable for their long cycle life, rapid charge−discharge rates, and high power density.[1−3] Electric double-layer capacitors (EDLCs) store energy through reversible ion adsorption at the electrode/electrolytes interface, a process faster than the Faradaic reactions in batteries.[3−5] However, the adsorption process limits the energy density in EDLCs.[6,7] To enhance the performance, innovations in both electrodes and electrolytes are crucial. The integration of porous electrodes with ionic liquid (IL) electrolytes has been shown to optimize capacitance.[8−15] With the growing demand for wearable electronics, flexible energy storage devices are increasingly required.[16−18] Replacing ILs with polyelectrolytes (PEs) enhances flexibility and prevents leakage. PEs, which contain ionizable groups in their chains, offer several advantages, including low cost, high capacitance, good mechanical properties, and ease of processing.[19−23] Consequently, PEs are expected to play a pivotal role in advanced energy storage technologies.

Progress in IL-based capacitors has been driven by a deeper understanding of molecular adsorption behavior.[24−26] Simulation techniques, such as the constant potential method (CPM), have significantly contributed to this knowledge.[27−29] Compared to ILs, PEs exhibit more complex electrochemical behavior.[30,31] First, as polymer materials, PE chains display versatile and dynamic conformations that vary with their distance from the electrode surface. Second, the distribution of charged beads along a polymer chain, or charge sequence, affects adsorption and, consequently, the performance of EDLCs. With these differences, whether insights from ILs systems apply directly to PEs remains uncertain, highlighting the need for fundamental research.

The adsorption of PEs on oppositely charged surfaces has been extensively studied over the past few decades.[31−35] These studies have identified patterns of how the charge properties of PEs influence their adsorption behavior. First, a higher charge fraction generally leads to stronger adsorption as the electrostatic energy of the electric double layer (EDL) in PE solutions confined between two charged surfaces increases with the charge fraction.[36] However, in some cases, the amount of adsorbed PE exhibits a nonmonotonic dependence on the charge fraction, initially increasing and then decreasing. This complex behavior is attributed to the shielding effect of

Received: March 4, 2025
Revised: June 9, 2025
Accepted: June 13, 2025
Published: June 19, 2025

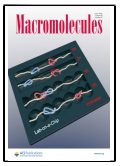

https://doi.org/10.1021/acs.macromol.5c00595
Macromolecules 2025, 58, 6883−6896

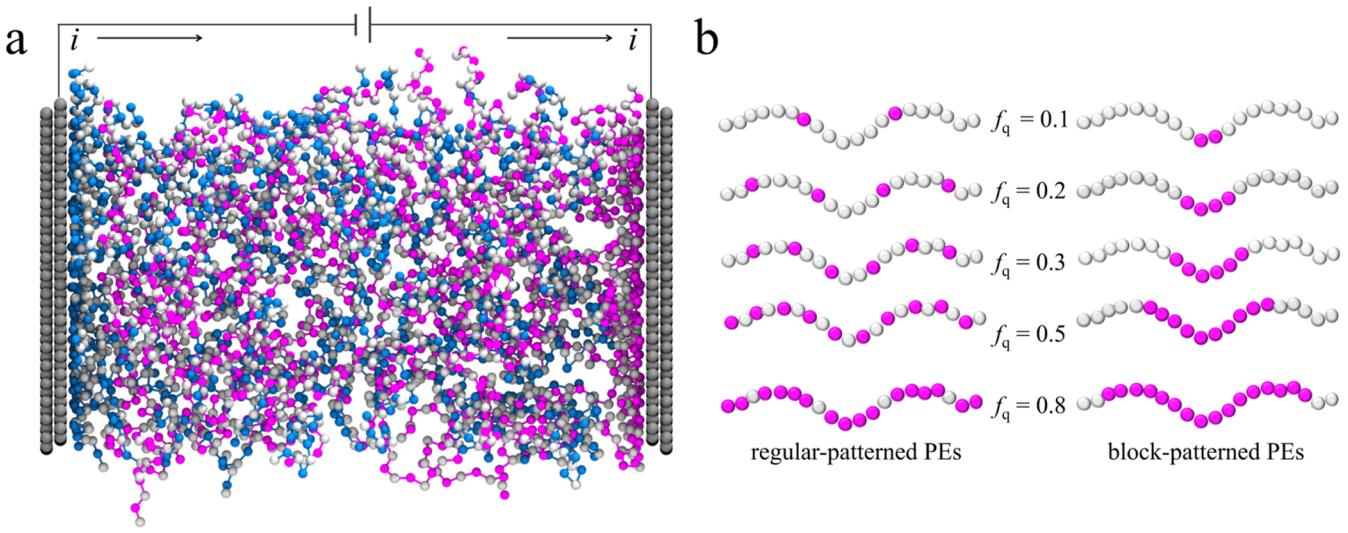

Figure 1. Electric double-layer capacitors (EDLCs) with PE solution as working electrolytes. (a) Snapshot of PE solution confined between two planar electrodes. The charge fraction of the PE is f_q = 0.5. The blue beads represent positively charged beads in polycation (PC) chains, the pink beads represent negatively charged beads in polyanion (PA) chains, the silver beads represent neutral beads, and the gray beads represent electrode beads. The distance between the two planar electrodes is fixed at 14.28 nm. (b) Schematic drawing of sequence of regular-patterned (charged beads are uniformly spaced along the chain) and block-patterned (charged beads at the chain's center) of PA chains with different charge fraction f_q.

counterions at high charge fractions.[37,38] Second, the charge sequence significantly impacts the adsorption process. Block copolymers with charged blocks show a greater effect on PE adsorption compared with alternating sequences. Additionally, increasing block size and reducing the number of blocks enhance adsorption.[38,39] Beyond adsorption, block size also affects other PE behaviors, such as coacervation[40−43] and response to stimuli.[44]

Despite recent advances, our understanding of how charge fractions and sequences affect capacitors containing PEs (PE) remains limited. In particular, the relationship between polymer adsorption on electrodes and EDLC (EDLC) performance, including capacity and charging rate, is not fully understood. Previous studies have shown that counterions complicate this analysis by significantly influencing the PE adsorption behavior. These counterions often obscure the effects of the charge fraction and sequence, making it difficult to isolate their individual roles. To address this issue, we used antisymmetric PEs composed of polycations (PC) and polyanions (PA) with identical charge patterns. Although this design is idealized, it eliminates the need for counterions, thereby eliminating their impact. In contrast, single PE solutions contain counterions. However, in mixtures of two PE solutions, the salt concentration can be independently controlled, for example, through dialysis.[41,42,45−48]

We employ molecular dynamics simulations to investigate how charge fraction and charge sequence influence the EDL and relate these findings to supercapacitor performance, including capacity and charging rate. By focusing on antisymmetric PEs, we aim to gain a clearer understanding of the intrinsic factors that govern polymer adsorption and their direct effects on the EDLC performance.

RESULTS AND DISCUSSION

Nanocapacitor with PE Electrolytes. We study a nanometer-scale capacitor composed of planar electrodes separated by polyelectrolyte (PE) solutions, as shown in Figure 1a. The PEs consist of PC and PA, achieving charge neutrality and eliminating the need for small counterions. This design simplifies the system, allowing us to focus on how PEs influence the capacitor performance. The electrode separation is H = 14.28 nm, significantly larger than in simulations of EDLCs with simple electrolytes solutions composed of small ions.[49,50] This large separation accounts for the longer correlation lengths inherent to polymeric PEs compared to those of simple ion solutions.

We model the PEs using a coarse-grained approach and treat the solvent implicitly as a dielectric medium with a dielectric constant of ε_r = 80. We employ the CPM, which maintains a constant electric potential difference between electrodes, allowing charge fluctuations to respond to local variations in electrolyte density.[51−56] Another common method is the constant charge method (CCM),[57,58] in which electrode atoms bear constant charges during the simulation. Although both methods exhibit similar equilibrium behavior for fast electrochemical processes[59] at low electric potential difference, the local charge fluctuations can lead to qualitatively differences between CPM and CCM at high voltages,[53] resulting in different double-layer relaxation times.[54,60] CPM simulations are typically performed with an explicit solvent. For our models with implicit solvent, we account for the solvent's dielectric effects by rescaling the charges and electric potentials (see section "charge and electric potential rescaling" in the Supporting Information). Specifically, charges are scaled by $1/\sqrt{\varepsilon_r}$ and electric potential difference by $\sqrt{\varepsilon_r}$.[61]

To explore the effects of the charge fraction (f_q) and charge sequence, we design two series of PE chains (Figure 1b). In the regular-patterned PEs, charged beads are uniformly spaced along the chain. In contrast, the block-patterned PEs concentrate charged beads at the chain's center, resembling a triblock copolymer. In experimental setups, solutions typically include a single type of PEs with their counterions. However, counterions introduce asymmetry and complicate the system, often masking the effects of charge fraction and sequence. To address this, we use fully antisymmetric PC and PA chains. These chains have identical lengths, charge fractions, and

https://doi.org/10.1021/acs.macromol.5c00595
Macromolecules 2025, 58, 6883−6896

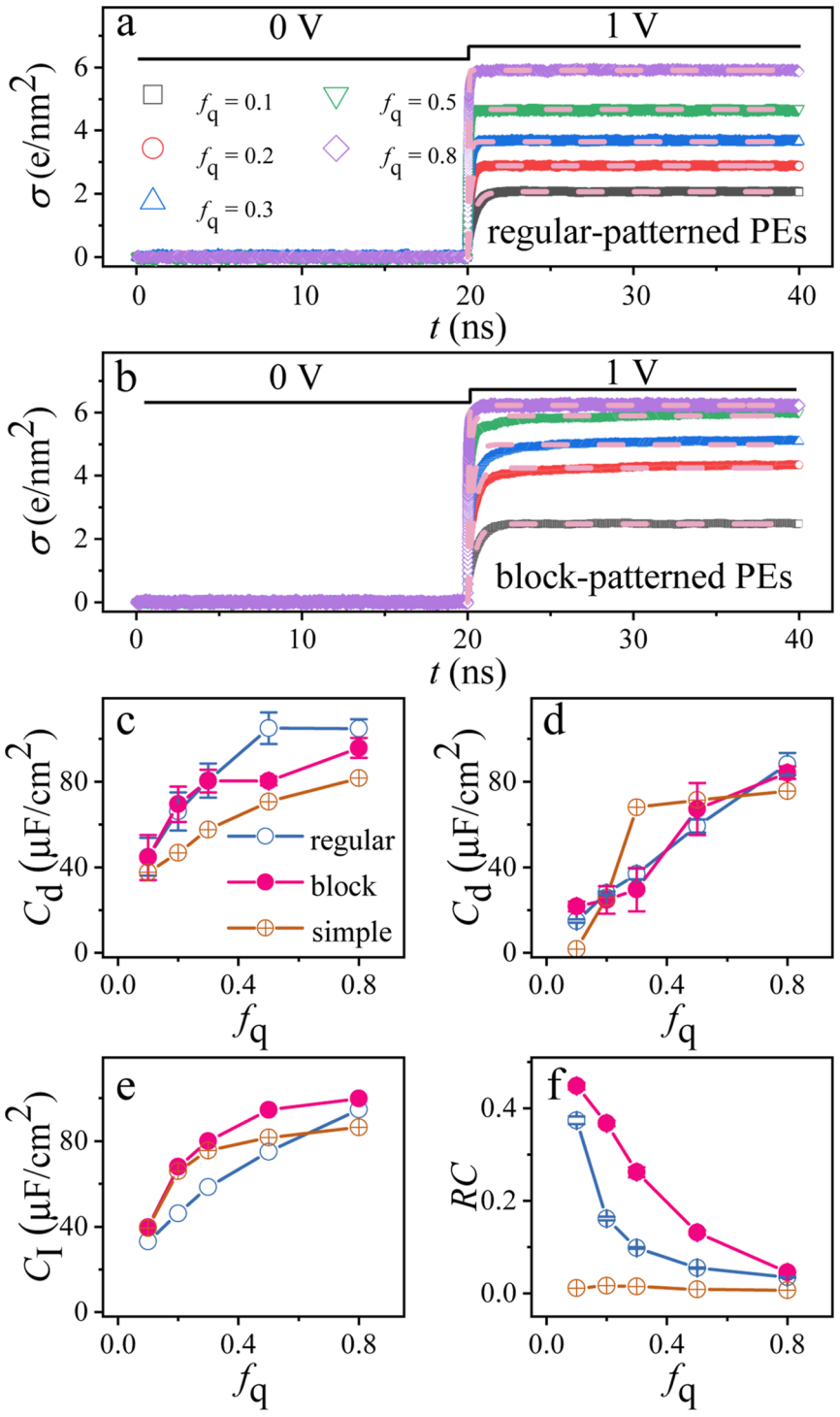

Figure 2. Performance of EDLC based on PE solutions. (a,b) Time evolution of the charge density (σ) on the positive electrode of EDLC with working PEs of regular-patterned PEs and block-patterned PEs. In the first 20 ns, the potential difference between two electrodes is 0 V. At 20 ns, the potential difference is set to 1 V. Pink dashed lines are exponential fitting curves, $\sigma(t) = \sigma_{max}(1 - e^{-t/RC})$. The (c,d) differential capacitance C_d with $\delta\Psi$ = 0 V (c) and $\delta\Psi$ = 1 V (d) with working electrolytes of regular-patterned PE, block-patterned PE, and simple electrolyte. The (e) integral capacitance C_I for with $\delta\Psi$ = 1 V with working electrolytes of regular-patterned PE, block-patterned PE, and simple electrolyte. The (f) charging relaxation time constant RC for EDLC's with working electrolytes of regular-patterned PE, block-patterned PE, and simple electrolyte. Error bars represent the standard deviation from four independent measurements in panels (c−e).

charge patterns, eliminating counterion effects. This approach allows us to isolate the influence of charge fraction and sequence on adsorption and, consequently, on EDLC performance. For comparison, we also examine EDLCs based on simple electrolytes with small ion solutions. These electrolytes contain the same number of charged and neutral beads as the PE systems, matching their charge fractions. Further details are provided in the Methods section.

Energy Storage Performances. We evaluate the performance of EDLCs by examining their capacity and charging rate

https://doi.org/10.1021/acs.macromol.5c00595
Macromolecules 2025, 58, 6883−6896

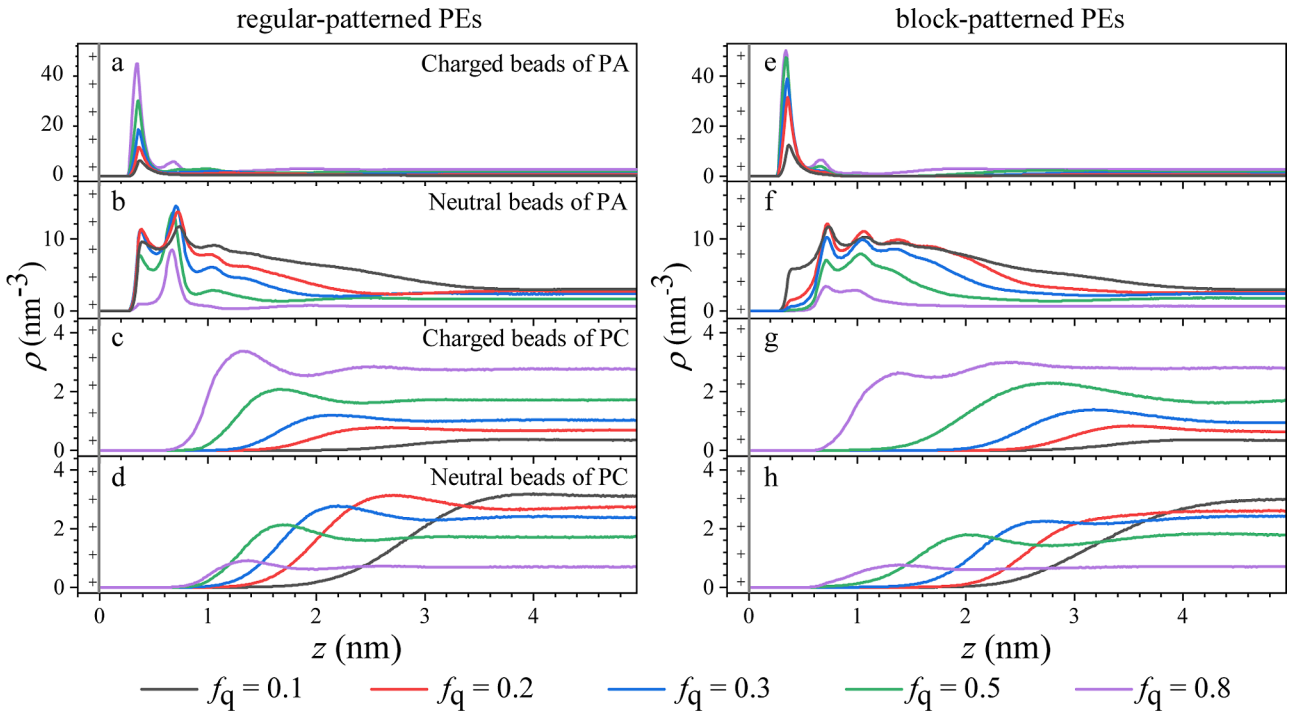

Figure 3. EDLC structure characterized by number density of different components along the normal direction of the electrode surface. z is the distance from the outmost layer of atoms of the positive electrode. The left panels and right panels are for EDLCs with regular-patterned and block-patterned PEs, respectively. (a,e) Charged beads of polyanion chains. (b,f) Neutral beads of polyanion chains. (c,g) Charged beads of polycation chains. (d,h) Neutral beads of polycation chains.

with different PEs. For each EDLC, we first simulate for 20 ns at an electric potential difference of $\Delta\Psi = 0$ V. After 20 ns, we stepwise increase the potential difference to 1 V to study the charging process. Figure 2a,b shows the variation of positive electrode charge density, σ, over time. At $\Delta\Psi = 0$ V, the electrode charges fluctuate around $\langle\sigma\rangle = 0$ e/nm^2. This occurs because we use an antisymmetric setup of PEs, resulting in a potential of zero charge, $\Psi_{PZC} = 0$ V. Breaking the antisymmetry between PC and PA chains can shift Ψ_{PZC} away from 0 V, which is another interesting topic for future research. After $\Delta\Psi$ increases to 1 V, σ rises, until it reaches a steady-state plateau.

In experimental studies, the differential capacitance (C_d) is defined as the derivative of the electrode charge (Q) with respect to the electrode potential ($\Delta\Psi$) at equilibrium, $C_d = \frac{d\langle Q\rangle}{d\Delta\Psi}$, where the electrode charge is expressed as $Q = A\sigma$, with A being the electrode area and σ the charge density on the electrode surface. Physically, C_d describes the sensitivity of the electrode's stored charge to variations in the applied potential. In molecular simulations, C_d is typically computed from the equilibrium fluctuations of the electrode charge:[50,62] $C_d = \beta\langle\delta Q^2\rangle$, where $\delta Q = Q - \langle Q\rangle$ represents fluctuations of the charge around its equilibrium mean value, and $\beta = 1/(k_B T)$ with k_B the Boltzmann constant and T the absolute temperature. This statistical definition provides a direct computational route to assessing the differential capacitance from equilibrium simulations.

Figure 2c summarizes the areawise differential capacitance. Generally, increasing the charge fraction of PEs enhances C_d due to more charged species in the electrolyte. This trend is consistent with EDLCs using simple electrolytes as working electrolytes.[15] Within the scope of our model, EDLCs with simple electrolytes exhibit slightly lower C_d values, suggesting that PEs can improve the EDLC capacitance.

Differential capacitance typically varies with $\Delta\Psi$, showing increases, decreases, or nonmonotonic behavior depending on the electrolyte.[63] Due to computational intensity, we do not construct the full C_d versus $\Delta\Psi$ curve. However, as shown in Figure 2c and d, C_d at $\Delta\Psi = 1$ V is smaller than that at $\Delta\Psi = 0$ V. This aligns with camel-shaped or bell-shaped C_d–$\Delta\Psi$ curves, where capacitance decreases as electric potential rises.

Comparing C_d for EDLCs with regular-patterned and block-patterned charge sequences, we find minimal differences when $f_q \leq 0.3$. At higher charge fractions, however, block-patterned PEs exhibit slightly lower C_d at 0 V compared with regular-patterned PEs, suggesting that sequence effects become significant at elevated charge fractions. At $\Delta\Psi = 1$ V (Figure 2d), the differences diminish, possibly because ion-exclusion effects dominate capacitance at high potentials,[64] overshadowing the influence of charge sequences. This is also supported by the fact that EDLCs based on PEs show C_d values comparable to those of EDLCs based on simple electrolytes. These findings suggest that while charge sequence has a noticeable impact at lower potentials and higher charge fractions, its effect becomes less pronounced at higher potentials.

Integral capacitance C_I is a more relevant parameter for assessing the overall energy storage ability of a capacitor. C_I is calculated as $C_I = \frac{Q}{\Delta\Psi - \Delta\Psi_{PZC}}$, where $\Delta\Psi_{PZC}$ is the point of zero charge and is 0 V in our antisymmetric PE systems. As shown in Figure 2e, EDLCs with block-patterned PEs exhibit larger C_I values compared to those with regular-patterned PEs or simple electrolytes. This indicates that block-patterned PEs are more effective in enhancing the energy storage capability of EDLCs. In contrast, regular-patterned PEs generally show lower C_I values than simple electrolytes except at a charge fraction of f_q

https://doi.org/10.1021/acs.macromol.5c00595
Macromolecules 2025, 58, 6883−6896

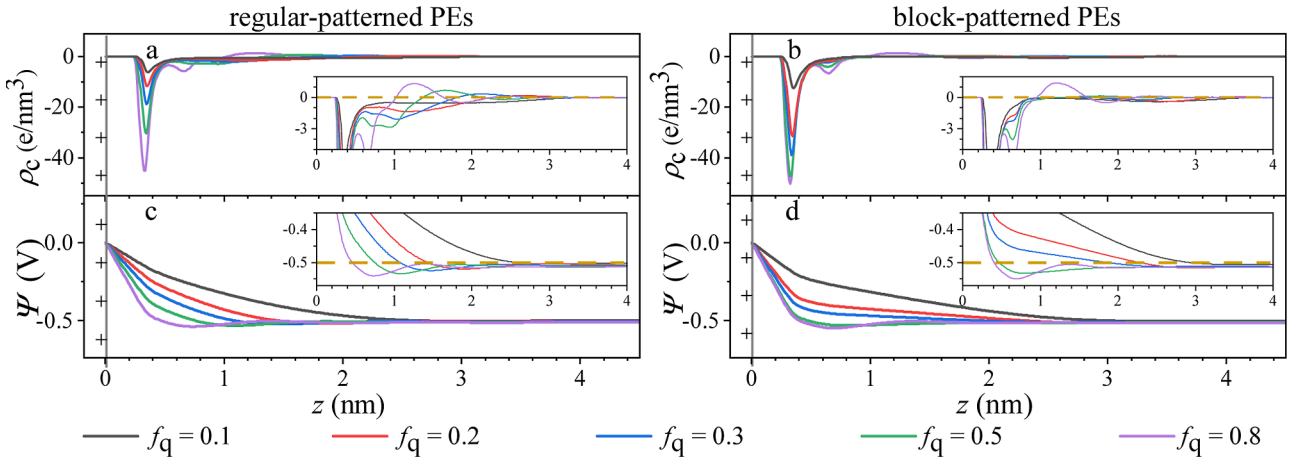

Figure 4. EDLC structure characterized by net charge density profiles $\rho_C(z)$ and potential profiles $\Psi(z)$ of different components along the normal direction of the electrode surface. z is the distance from the outmost layer of atoms of the positive electrode. The left panels (a,c) and right panels (b,d) are for EDLCs with regular-patterned and block-patterned PEs, respectively. The (a,b) net charge density profiles of regular-patterned PE chains (a) and block-patterned PE chains (b). Insets magnify $\rho_C(z)$ near the positive electrode. The charge density curves exhibit negative charge accumulation near the positive electrode, and increasing f_q leads to greater negative charge buildup and a sharp drop in potential near the electrode surface. Co-ion adsorption occurs beyond two layers of counterion adsorption (overscreening). The (c,d) electric potential profiles, $\Psi(z)$, of regular-patterned PE chains (c) and block-patterned PE chains (d). The insets magnify $\Psi(z)$ near the positive electrode. $\Psi(z)$ is obtained by solving Poisson's equation in the z-direction. A dip (overscreening) below the bulk potential becomes pronounced at higher f_q.

= 0.8. Notably, regular-patterned PEs with f_q = 0.8 contain some charged blocks. This suggests that the presence of charged blocks enhances the EDLC capacitance.

To examine the charging process, we apply a potential of 1 V and quantify the charging rate by fitting the $\sigma(t)$ curve to an exponential function:[50] $\sigma(t) = \sigma_{max}(1 - e^{-t/RC})$, where RC is the relaxation time of an equivalent circuit with one capacitor (C) and one resistor (R) in series. As shown in Figure 2f, EDLCs based on PEs exhibit significantly larger RC values compared with those using simple electrolytes. This increase suggests that the connectivity among charged species in PEs hinder their movement toward the electrodes, thereby slowing the charging process. RC decreases with increasing f_q for both block-patterned and regular-patterned PEs. Higher charge fractions enhance the interactions between the electrode and oppositely charged PE chains, resulting in higher charging rates. Notably, regular-patterned PEs show smaller RC values than block-patterned PEs, indicating that a uniform charge distribution facilitates more rapid charging. Moreover, capacitors with regular-patterned PEs closely follow the exponential charging curve, suggesting a single dominant relaxation process. In contrast, capacitors with block-patterned PEs deviate from this behavior at $f_q \geq 0.2$, displaying slower charging rates. These curves are better fitted by a stretched exponential function, or Kohlrausch–Williams–Watts (KWW) function,[65−67] $\sigma(t) = \sigma_{max}(1 - e^{-(t/\tau)^{\beta}})$, where β quantifies the degree of stretchness (Figures S2 and S3 and Tables S2–S4). The stretching exponent β lies in the range $0 < \beta \leq 1$. A value of β = 1 corresponds to a single-exponential decay (Debye-like behavior), while $\beta < 1$ indicates a distribution of relaxation times, reflecting increasing dynamical heterogeneity or complexity in the system. The β values for regular-patterned PEs range from 0.67 to 0.80 across different charge fractions, while those for block-patterned PEs fall between 0.62 and 0.75. The KWW function effectively fits these curves and exhibits lower β values (Tables S2 and S3), indicating that the charging process of EDLCs with block-patterned PEs involves multiple relaxation processes. This complexity likely arises from the intricate adsorption patterns and conformational dynamics of the block-patterned PE chains, as discussed in subsequent sections. The electrodes are modeled as ideal conductors, rendering the inclusion of a Thomas-Fermi screening length unnecessary.

Electric Double-Layer Structure. The performance of EDLCs primarily depends on the EDL formed at the electrode–electrolyte interface.[68−70] To investigate this, we examined the EDL structure in our nanocapacitor with PE electrolytes. Figure 3 displays key density profiles along the electrode normal, focusing on the EDL near the positive electrode with the outermost layer located at z = 0 nm. Due to the antisymmetric design of our polycation (PC) and polyanion (PA) chains, the EDL near the negative electrode is a mirror image of that near the positive electrode, with the PC and PA profiles interchanged.

Across different PE chains varying in charge fraction (f_q) and charge sequence, the EDL structures remain consistent. Specifically, PA chains adsorb onto the positive electrode through electrostatic attraction, while PC chains are repelled, creating a depletion layer of PC chains near the positive electrode. The thickness of this depletion layer depends on the charge fraction and sequence pattern.

For both regular-patterned and block-patterned sequences, increasing the charge fraction (f_q) enhances the adsorption of PA chains onto the positive electrode. This enhancement is evident from higher first peak magnitudes and closer peak positions in the density profiles of charged beads (Figures 3a,e and S4a,b). A higher charge fraction also strengthens the binding between PA and PC chains, allowing the peak positions of PC chains to approach the electrode more closely (Figures 3c,g and S4c,d).

Comparing regular-patterned and block-patterned charge sequences, block-patterned PA chains exhibit higher first peak densities of charged beads, and their first peak positions are closer to the electrode surface than those of regular-patterned PA chains at the same charge fraction f_q (Figure S4a). These observations indicate that block-patterning enhances the

https://doi.org/10.1021/acs.macromol.5c00595
Macromolecules 2025, 58, 6883−6896

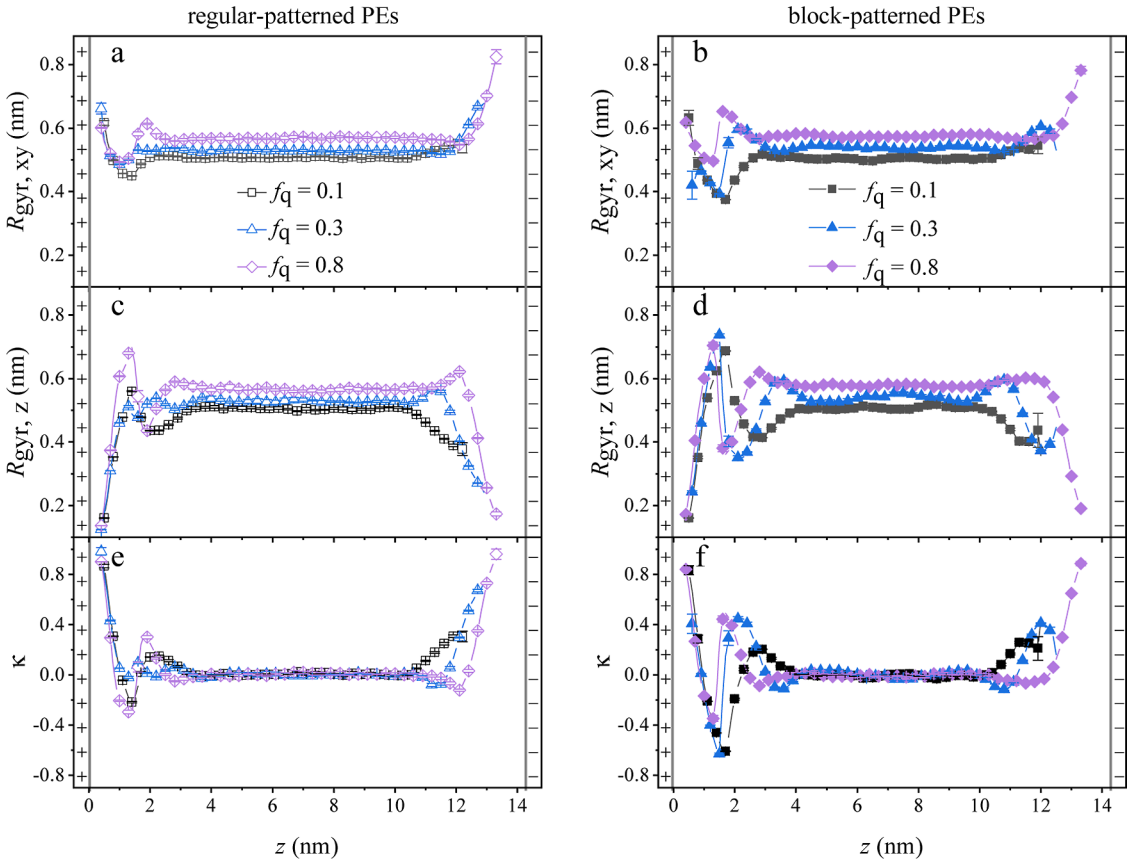

Figure 5. PE chains conformation in the EDLC. The chain conformation is characterized by radius of gyration in plane parallel to the electrode surface ($R_{gyr,xy}$) and in direction perpendicular to the electrode surface ($R_{gyr,z}$), and oblateness derived from them, κ (eq 2). To reflect the inhomogeneity in the EDLC, chain conformations at different locations are analyzed. (a,b) $R_{gyr,xy}$ for regular-patterned (a) and block-patterned (b) chains. (c,d) $R_{gyr,z}$ for regular-patterned (c) and block-patterned (d) chains. Near the electrode, PE chains are compressed in the direction perpendicular to the electrode surface and extended parallel to it. The (e,f) oblateness, κ, for regular-patterned (e) and block-patterned (f) chains. The oscillation of κ around 0 reflects that the chains first compress and then elongate along the normal direction of the electrode surface.

adsorption strength of PEs on oppositely charged electrodes, consistent with previous studies.[38]

At high charge fractions, neutral beads are less likely to appear in the first adsorption layer (Figure 3b,f), especially for block-patterned PA chains. When $f_q \geq 0.5$, the first adsorption layer of block-patterned PA chains is almost entirely composed of charged beads. This suggests that in block-patterned PEs, the first layer of adsorbed PA chains predominantly consists of charged beads, whereas regular-patterned PEs have a mixture of neutral and charged beads. The separation of charged and neutral beads along the chain in block-patterned PEs allows for greater segregation within the same chain compared with regular-patterned PEs. As discussed in subsequent sections, block-patterned PE chains can have their charged blocks adsorbed onto the electrode surface while leaving neutral blocks extended into the electrolyte, forming tail structures. This structural arrangement likely contributes to the higher integral capacitance observed with block-patterned PEs (Figure 2e). Furthermore, this separation requires additional conformational adjustments during charging, resulting in slower charging kinetics (Figure 2f) and the introduction of multiple relaxation processes. Consequently, block-patterned PEs exhibit Kohlrausch−Williams−Watts (KWW) type charging kinetics (Figure 2b), indicating a more complex relaxation behavior. These findings reveal that charge sequence significantly affects both the EDL structure and the adsorption dynamics in EDLCs, which in turn influences the capacitance and charging rate.

To gain deeper insight into the EDL structure, we analyze the net charge distribution $\rho_C(z)$ along the electrode normal. By solving Poisson's equation in the z-direction, we further obtain the electric potential profiles $\Psi(z)$

$$\frac{\partial^2 \Psi(z)}{\partial z^2} = -\frac{\rho_C(z)}{\varepsilon_0 \varepsilon_r} \tag{1}$$

where ε_0 is the vacuum permittivity and ε_r is the solvent dielectric constant. We apply boundary conditions of $\Psi(0) = 0$ V and $\Psi'(H/2) = 0$ V/m. Owing to the antisymmetry between polycation (PC) and polyanion (PA) chains, the profiles near the positive and negative electrodes are mirror images. Therefore, we focus on the region near the positive electrode at $z = 0$ nm.

Charge density profiles reveal an accumulation of negative charges near the positive electrode, leading to a decrease in electric potential $\Psi(z)$ in this region (Figures 4 and S6). For both regular-patterned and block-patterned PEs, increasing the charge fraction f_q results in a more negative charge accumulation and a steeper decline in the electric potential near the electrode surface. We can characterize the EDL thickness as the distance from the electrode where $\Psi(z)$ reaches the bulk potential $\Psi_{bulk} = -0.5$ V, marking the end of charge separation. The EDL thickness is generally less than 4

https://doi.org/10.1021/acs.macromol.5c00595
Macromolecules 2025, 58, 6883−6896

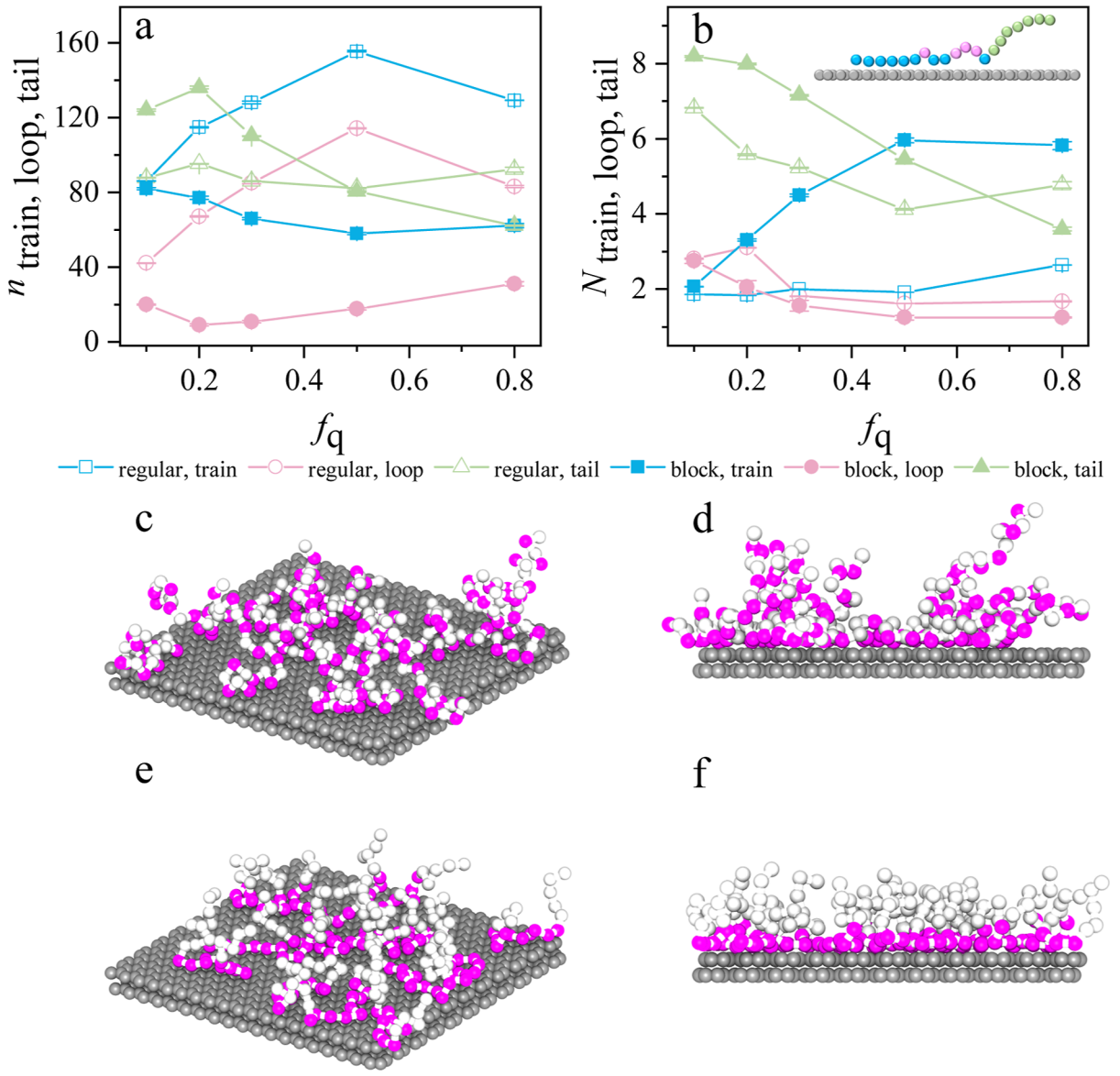

Figure 6. Conformation of adsorbed PE chains are characterized by the number of chain fragments with train, loop, or tail features. The (a) average number n of train, loop, and tail fragments. The (b) average length N of train, loop, and tail fragments. The inset shows the illustration of train (blue beads), loop (pink beads), and tail (green beads) fragments. Block-patterned PEs have fewer but longer train fragments, indicating larger contiguous chain fragments that enhance adsorption strength. (c,d) Top view (c) and side view (d) of regular-patterned PEs with a charge fraction $f_q = 0.5$. (e,f) Top view (e) and side view (f) of block-patterned PEs with a charge fraction $f_q = 0.5$. To better illustrate the conformations of PE chains adsorbed on the electrode surface, not all the adsorbed chains are shown in (c–f).

nm and decreases with increasing f_q, consistent with the trends observed in the density profiles in Figure 3.

Overscreening[71,72] occurs at high charge fractions in all three electrolytes studied. Overscreening typically arises under conditions of high electrode surface charge, high ion valence or concentration, or a low dielectric constant. In our charge distribution profiles, overscreening manifests as charge inversion due to co-ion adsorption after the initial counterion layer. In the electric potentials profile, it appears as a dip below the bulk potential, resulting in a nonmonotonic $\Psi(z)$ profile away from the electrode surface.

At low charge fraction (e.g., $f_q = 0.1$), overscreening is absent. The electric potential $\Psi(z)$ decreases monotonically from 0 V at $z = 0$ nm to $\Psi_{bulk} = -0.5$ V, and there is no region where $\rho_C(z) > 0$ e/nm^3, within the allowance of errors of the density profiles. This behavior stems from the low concentration of ionizable species, resembling dilute liquid electrolytes.[31,73] At higher charge fractions, overscreening becomes evident. We observe positive charge regions in the charge density profiles (Figure 4a,b) and nonmonotonic variations in $\Psi(z)$ (Figure 4c,d). The extent of overscreening increases with f_q. Notably, for simple electrolytes, overscreening appears only at a high charge fraction of $f_q = 0.8$, whereas for PE electrolytes, it is already evident at $f_q \geq 0.2$. This suggests that overscreening is more likely to occur in PE electrolytes, likely due to the connectivity of charges along the polymer chains, which leads to stronger correlations among the charged beads. The enhanced overscreening in PE electrolytes can explain the higher differential capacitance at 0 V observed in EDLCs with these electrolytes (Figure 2c). At a larger potential of 1 V, however, the benefits from overscreening are outweighed by size-exclusion effects, making the differential capacitance

https://doi.org/10.1021/acs.macromol.5c00595
Macromolecules 2025, 58, 6883–6896

comparable among all three electrolytes (Figure 2d).[64] Regular-patterned PEs exhibit stronger overscreening compared to that of block-patterned PEs. This arises because, in regular-patterned chains, neutral beads consistently accompany charged beads upon adsorption, reducing the local effective dielectric constant near the electrode surface. Such a reduced dielectric environment enhances electrostatic correlations, thereby promoting more pronounced overscreening.

Conformation. As demonstrated in previous sections, the connectivity and flexibility of PE chains impart unique properties to EDLCs.[31] Understanding the conformations of PE chains near electrode surfaces is essential to elucidate how chain connectivity influences the EDL structure and, consequently, the performance of EDLCs. To gain deeper insight into these effects, we analyze the chain conformations near the electrodes.

Figure 5a–d presents the components of the radius of gyration for polyanion (PA) chains in directions parallel ($R_{gyr,xy} = (R_{gyr,x} + R_{gyr,y})/2$) and perpendicular ($R_{gyr,z}$) to the electrode surface, plotted against the position z between the positive electrode at $z = 0$ nm and the negative electrode at $z = 14.28$ nm. In the central region of the EDLC, far from both electrodes, $R_{gyr,xy}$ and $R_{gyr,z}$ remain constant and independent of z. This indicates that the chains adopt bulk-like conformations in this region, consistent with the flat density profiles observed earlier. It also suggests that the distance between the electrodes is sufficient to avoid nanoconfinement effects on the EDLC behavior.[50] For both regular-patterned and block-patterned sequences, the overall radius of gyration increases with charge fraction f_q due to enhanced intrachain electrostatic repulsion, which causes the chains to expand.

Near the positive electrode, $R_{gyr,xy}$ increases while $R_{gyr,z}$ decreases compared to the bulk values (Figure 5a–d). This suggests that the chains are compressed in the direction normal to the electrode surface and extended parallel to it, adopting an oblate conformation. Notably, the values of $R_{gyr,z}$ near the electrode are approximately 0.2 nm, comparable to the size of a monomer unit, and show little dependence on the charge fraction. This indicates that the PA chains are strongly adsorbed onto the electrode surface, lying almost flat with minimal extension in the z direction.

To quantify the degree of chain flattening, we define the oblateness parameter κ

$$\kappa = \frac{3(R_{gyr,xy} - R_{gyr,z})}{2R_{gyr,xy} + R_{gyr,z}} \quad (2)$$

where $\kappa = 0$ corresponds to an ideal spherical coil, positive values indicate oblate (flattened) shapes, and negative values indicate prolate (elongated) shapes. As shown in Figure 5e,f, κ reaches values of around 0.8 near the electrode for both charge sequences, confirming the oblate conformation of the adsorbed chains. This oblateness is relatively independent of the charge fraction, suggesting a consistent flattening effect due to strong adsorption.

Moving away from the electrode, both $R_{gyr,xy}$ and $R_{gyr,z}$ gradually return to their bulk values, and the oblateness parameter decreases. Notably, there is a region around $z = 1$ nm where κ becomes negative, indicating that the chains adopt a prolate shape elongated in the z direction. This transition from oblate to prolate conformations reflects the balance of electrostatic and entropic forces as the chains adjust their structures to minimize intrachain and interchain repulsions while accommodating spatial constraints.[36,74,75]

Comparing the regular-patterned and block-patterned charge sequences, block-patterned PEs exhibit more pronounced variations in the chain conformation near the electrode surface. The stronger flattening and subsequent elongation suggest that block-patterned chains undergo more significant conformational adjustments due to their concentrated charge segments. This behavior is consistent with the larger density profile variations observed for block-patterned PAs near the positive electrode (Figure 3), indicating stronger electrostatic correlations in these systems. As block-patterned PEs require more time to establish these conformational changes, this contributes to the slower charging dynamics and higher RC values compared with regular-patterned PEs (Figure 2f).

To gain deeper insight into the adsorption behavior, we examined the configurations of the adsorbed chains, classifying them into trains, loops, and tails (Figure 6). Trains are sequences of monomers directly in contact with the electrode surface; loops are segments that extend away from the surface but reconnect to the surface; tails are chain ends that extend into the bulk without returning (see the illustration in the inset of Figure 6b).

In Figure 6a, we observe that block-patterned PEs have fewer train segments compared with regular-patterned PEs, but the trains are longer (Figure 6b). This implies that block-patterned chains tend to adsorb onto the electrode surface in larger contiguous segments. The concentrated charged blocks enhance the adsorption strength, leading to fewer but longer train segments. This stronger and more extensive adsorption likely contributes to the higher integral capacitance observed with block-patterned PEs as it facilitates more effective charge accumulation at the electrode interface.

The average loop length is similar for both charge patterns, around two monomer units (Figure 6b), suggesting that the chains are tightly adsorbed onto the electrode with minimal looping. However, block-patterned PEs exhibit fewer loop structures than regular-patterned PEs, reinforcing the notion of stronger and more direct adsorption in block-patterned sequences. The reduced number of loops may enhance the stability of the EDL, potentially improving the capacitor's performance.

Regarding tails, regular-patterned PEs show little dependence on the charge fraction f_q in both the number and length of tails. In contrast, block-patterned PEs display a decrease in both the number and length of tails as f_q increases. As shown in the following section, the difference in the trend of the number of tails results from the fact that the steady-state number of adsorbed PE chains remains constant with increasing f_q values for regular-patterned PEs but decreases for block-patterned PEs. This suggests that at higher charge fractions, block-patterned PEs achieve stronger adsorption with fewer chains (Figure 6c–f and Movie S1). While this enhances the capacitance due to more effective charge accumulation, it may also result in slower charging rates because the chains undergo more significant conformational adjustments during charging.

PE Adsorption Dynamics. Understanding the adsorption and desorption rates of PE chains on electrode surfaces is essential for elucidating the charging dynamics of the electrodes.[37,76,77] We consider a PE bead to be adsorbed if its distance from the outermost layer of the electrode is less

https://doi.org/10.1021/acs.macromol.5c00595
Macromolecules 2025, 58, 6883–6896

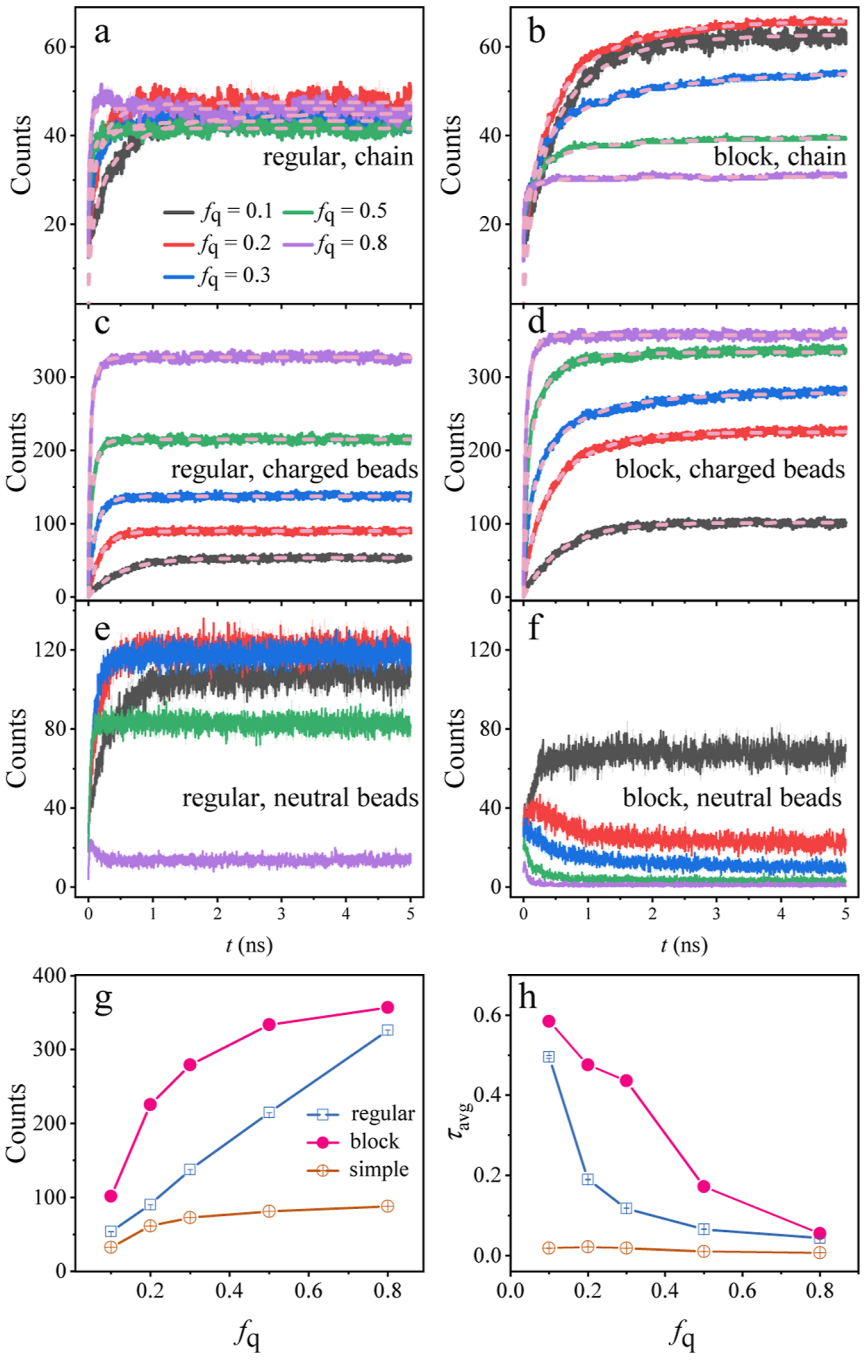

Figure 7. Time evolution of adsorption counts of PE chains (all beads), charged beads, and neutral beads at a potential of $\delta\Psi$ = 1 V. (a,b) Time evolution of adsorption counts for adsorbed chains with working electrolytes of regular-patterned PEs and block-patterned PEs. Pink dashed lines are KWW fitting curves. Leveling off indicates saturation of available adsorption sites on the electrode surface. Regular-patterned PEs are almost independent of charge fraction, while block-patterned PEs are highly dependent on the charge fraction. (c,d) Adsorbed charged beads. Pink dashed lines are KWW fitting curves. Higher charge fractions result in increased adsorption counts and faster adsorption dynamics. (e,f) Adsorbed neutral beads. The apparent contrast of neutral beads reveals the conformational rearrangement of the block-patterned PEs and brings about a complex relaxation process. The (g,h) equilibrate adsorption amount and average relaxation time, $\tau_{avg} = \frac{\tau}{\beta}\Gamma\left(\frac{1}{\beta}\right)$ of adsorbed charged beads for regular-patterned PEs, block-patterned PEs, and simple electrolyte. Clustering of charges within the chains enhances adsorption efficiency. Error bars represent the standard deviation from four independent measurements in panels (g,h).

than the cutoff distance l_{cut}. A polymer chain is considered adsorbed if any of its beads meets this criterion. Here, we set l_{cut} = 0.5 nm, corresponding to the first minimum in the density profiles of PE beads near oppositely charged electrodes (see Figure 3b,f). Although this minimum varies slightly with different charge fractions (f_q) and charge sequences, using a common cutoff minimizes inconsistencies due to varying thresholds.

After a potential of 1 V is applied, Figure 7a,b shows that the number of adsorbed chains increases rapidly before reaching a plateau. This rapid initial adsorption is driven by electrostatic attraction between the charged beads on the PE chains and the

https://doi.org/10.1021/acs.macromol.5c00595
Macromolecules 2025, 58, 6883−6896

oppositely charged electrode. The subsequent leveling off indicates saturation of available adsorption sites on the electrode surface, leading to a steady-state equilibrium. Charged beads (Figure 7c,d) exhibit significantly higher adsorption counts compared with neutral beads (Figure 7e,f). This disparity reflects the direct electrostatic interactions that promote adsorption of charged beads, while neutral beads are adsorbed mainly due to chain connectivity and entropic factors.

For both regular-patterned and block-patterned PEs, higher charge fractions result in the increased adsorption amount (Figure 7g) and faster adsorption dynamics (Figure 7h) for charged beads. This trend underscores the role of electrostatic attraction in driving adsorption: increasing f_q enhances the overall charge on the PE chains, strengthening their interaction with the electrode. Notably, the block-patterned charge sequence amplifies this effect, particularly at high charge fractions, suggesting that the clustering of charges within the chains enhances the adsorption efficiency.

In the case of regular-patterned PEs, the number of adsorbed chains shows minimal dependence on the charge fraction (Figure 7a), with equilibrium adsorption levels remaining relatively constant across different f_q. Conversely, block-patterned PEs display a strong dependence on the charge fraction (Figure 7b), where higher f_q leads to a decreased number of adsorbed chains. This behavior can be explained by considering the train, loop, and tail configurations of the adsorbed chains (Figure 6). In block-patterned PEs, increasing f_q results in more strongly charged blocks within the chains. These extended charged segments have a stronger affinity for the oppositely charged electrode, forming longer training segments upon adsorption (Figure 6b). As each chain's charged block occupies more surface area due to the increased train length, fewer chains are needed to cover the electrode surface. Consequently (Figure 6e,f), the total number of adsorbed chains decreases as f_q increases. In contrast, regular-patterned PEs have charges distributed uniformly along the chain. Increasing f_q in these chains does not significantly alter the length of individual charged blocks or their adsorption behavior. The adsorption sites on the electrode are occupied by multiple chains with relatively constant train lengths (Figure 6b), resulting in a relatively constant number of adsorbed chains across different f_q. This explanation underscores the significant role of the charge sequence in determining adsorption behavior.

Another interesting observation arises with the adsorption dynamics of neutral beads in block-patterned PEs. For charge fractions $f_q \geq 0.2$, there is a decrease in the number of adsorbed neutral beads during the initial 2 ns, even as the number of adsorbed charged beads increases (Figure 7e,f). This contrasts with regular-patterned PEs, where the number of adsorbed neutral beads increases alongside the charged beads (Figure 7a,c). This differing trend suggests a change in the conformation of the adsorbed chains in block-patterned PEs during the initial charging stage. Specifically, as shown in previous sections, at steady state, the charged blocks of the chains tend to adsorb onto the electrode surface, while the neutral blocks extend away from the electrode into the electrolyte. As the charged segments attach to the electrode, the neutral segments are displaced, leading to a temporary decrease in the number of adsorbed neutral beads. This conformational rearrangement reflects the chain's effort to optimize electrostatic interactions while minimizing unfavorable contacts. This process contributes to the complexity of the charging dynamics in block-patterned PEs. The separation of charged and neutral blocks requires additional conformational adjustments, introducing multiple relaxation processes. As a result, the adsorption dynamics deviate from a simple exponential behavior (Figure S7) and are better described by the Kohlrausch–Williams–Watts (KWW) stretched exponential function (Figure 7a–d). Tables S5–S8 summarize the fitting parameters for regular-patterned and block-patterned PEs, revealing that the block-patterned configurations exhibit lower β values, indicating a broader distribution of relaxation times and a more complex adsorption process. This aligns with the observed KWW-type charging kinetics in electrode charge density (Figure 2b), indicating that the conformational dynamics of the PE chains play a significant role in the overall charging process. In contrast, regular-patterned PEs do not exhibit this decoupling of charged and neutral segments. The uniform distribution of charges along the chain leads to the simultaneous adsorption of both charged and neutral beads, resulting in adsorption dynamics that fit well to an exponential function. This suggests a more straightforward relaxation process without a significant conformational rearrangement. These findings highlight the importance of chain architecture in determining the adsorption behavior and charging dynamics. The ability of block-patterned PEs to form tail-like structures—with charged blocks adsorbed and neutral blocks extending into the solution—affects not only the adsorption kinetics but also the efficiency of charge storage and delivery. Understanding these conformational dynamics is crucial for optimizing the design of PEs in EDLC applications.

CONCLUSIONS

Our study sheds light on the fundamental role of charge fraction and charge sequence in PEs for EDLC applications. By employing antisymmetric PEs composed of PC and PA with identical charge patterns, we effectively eliminated the influence of counterions. This approach allowed us to focus on the intrinsic effects of the PEs themselves, providing a clearer understanding of how these macromolecules interact with electrode surfaces.

However, the advantages of block-patterned PEs come with trade-offs. While they improve capacitance, they also lead to slower charging rates. The concentrated charged segments in block-patterned PEs require more substantial conformational adjustments during adsorption onto the electrodes. This results in multiple relaxation processes, as evidenced by the Kohlrausch–Williams–Watts (KWW) type charging kinetics observed in our simulations. The need for the polymer chains to rearrange themselves contributes to longer charging times, highlighting a balance that must be struck between maximizing the capacitance and maintaining acceptable charging speeds. Our examination of the EDL revealed that both block-patterned and regular-patterned PEs promote enhanced overscreening compared with simple electrolytes, leading to increased charge accumulation near the electrode surface. This phenomenon enhances the local electric field and contributes to the higher capacitance observed. The conformational studies showed that while both types of PEs adopt flattened and oblate structures upon adsorption, block-patterned PEs arrange their charged blocks on the electrode surface with neutral blocks standing up and pointing away. This unique conformation enhances capacitance but requires additional time to establish, contributing to slower charging dynamics.

https://doi.org/10.1021/acs.macromol.5c00595
Macromolecules 2025, 58, 6883–6896

These findings have significant implications for the design of advanced energy storage materials. By careful selection of the charge fraction and sequence in PE electrolytes, it is possible to tailor the performance of EDLCs to meet specific application needs. For instance, applications requiring rapid charging might benefit from regular-patterned PEs, while those prioritizing maximum energy storage could utilize block-patterned PEs despite the slower charging rates. Future research could explore a wider variety of charge patterns and polymer architectures to further optimize the EDLC performance. Investigating the effects of chain length, degree of polymerization, and inclusion of functional groups could provide additional avenues for enhancing both capacitance and charging speed.

METHODS

The CPM iteratively optimizes atomic charges (represented as Gaussian distributions for computational tractability) to minimize the total energy of the system through a self-consistent process, with the applied potential difference ultimately introduced as a Lagrange multiplier in the formalism.[78] This approach allows for a realistic representation of the electrode−electrolyte interface, capturing the polarization response of electrodes with arbitrary nanostructures. This method has been used to calculate the differential capacitance of capacitors containing electrolytes, including ILs and PEs.[52−56] We utilize an improved CPM method[51] that allows concurrent execution of a "doubled cell" simulation to control the electrostatic potential between the positive and negative electrodes. This involves arranging two cells back-to-back with opposite polarities to create a zero-dipole supercell (Figure S1).

All our MD simulations were performed using the LAMMPS program.[79−81] In the coarse-grained molecular dynamics simulation, PEs are represented by linear bead−spring chains with regular-patterned or block-patterned charged beads, interconnected via a harmonic bond potential. The number of charged beads on the PE chain is governed by the charge fraction f_q (the ratio of charged beads to the total number of beads, each charged beads carrying an electron charge of $-e$ or $+e$), and the bead diameter is 0.35 nm. The chain length of the PE is fixed at 20. We investigated five charge fractions, f_q = 0.1, 0.2, 0.3, 0.5, and 0.8. The polycationic and polyanionic chains have identical lengths and charge distributions. We used 170 polyanion chains (n_{PA} = 170) and 170 polycation chains (n_{PC} = 170) to maintain the charge neutrality. The graphene electrode consists of two layers of hexagonally arranged carbon atoms, and the solvent is treated as a continuum background with a uniform dielectric constant ε_r = 80. While the implicit solvent model can influence the absolute values of calculated quantities, the relative trends among different PEs are expected to remain consistent. Weeks−Chandler−Andersen (WCA) terms are used to account for excluded volume interaction effects. The long-range Coulombic interaction is calculated by particle−particle particle-mesh (PPPM). The simple electrolyte is constructed with the same number of charged and neutral beads as the PE system, maintaining the same charge fraction, while all other simulation settings are kept identical to those of the PE system.

ASSOCIATED CONTENT

Data Availability Statement

All data needed to evaluate the conclusions in the paper are present in the paper and/or the Supporting Information.

Supporting Information

The Supporting Information is available free of charge at https://pubs.acs.org/doi/10.1021/acs.macromol.5c00595.

A single block-patterned polyelectrolyte chain adsorbing to the surface and relaxing to the optimal long-tail configuration (MP4)

Simulation methods, time evolution of the charge density of EDLC with working PEs of simple electrolytes; number density profile and net charge density profile along the normal direction of the electrode surface for simple electrolytes; and PE adsorption dynamics of regular-patterned PEs, block-patterned PEs, and simple electrolytes (PDF)

AUTHOR INFORMATION

Corresponding Author

Xian Kong − *South China Advanced Institute for Soft Matter Science and Technology, School of Emergent Soft Matter and Guangdong Provincial Key Laboratory of Functional and Intelligent Hybrid Materials and Devices, Guangdong Basic Research Center of Excellence for Energy and Information Polymer Materials, South China University of Technology, Guangzhou 510640, China;* orcid.org/0000-0001-5602-6347; Email: xk@scut.edu.cn

Authors

Yan Sui − *South China Advanced Institute for Soft Matter Science and Technology, School of Emergent Soft Matter, South China University of Technology, Guangzhou 510640, China*

Tingting Yin − *South China Advanced Institute for Soft Matter Science and Technology, School of Emergent Soft Matter, South China University of Technology, Guangzhou 510640, China*

Zixiao Yang − *South China Advanced Institute for Soft Matter Science and Technology, School of Emergent Soft Matter, South China University of Technology, Guangzhou 510640, China*

Yichun Zhao − *South China Advanced Institute for Soft Matter Science and Technology, School of Emergent Soft Matter, South China University of Technology, Guangzhou 510640, China*

Xiaoyu Kong − *South China Advanced Institute for Soft Matter Science and Technology, School of Emergent Soft Matter, South China University of Technology, Guangzhou 510640, China*

Dongluo Wu − *South China Advanced Institute for Soft Matter Science and Technology, School of Emergent Soft Matter, South China University of Technology, Guangzhou 510640, China*

Jiajia Zhou − *South China Advanced Institute for Soft Matter Science and Technology, School of Emergent Soft Matter and Guangdong Provincial Key Laboratory of Functional and Intelligent Hybrid Materials and Devices, Guangdong Basic Research Center of Excellence for Energy and Information Polymer Materials, South China University of Technology, Guangzhou 510640, China;* orcid.org/0000-0002-2258-6757

Xiupeng Chen − *South China Advanced Institute for Soft Matter Science and Technology, School of Emergent Soft Matter, South China University of Technology, Guangzhou 510640, China*

Complete contact information is available at: https://pubs.acs.org/10.1021/acs.macromol.5c00595

Author Contributions

Conceptualization: Xian Kong. Methodology: Yan Sui, Jiajia Zhou, Xiupeng Chen, and Xian Kong. Visualization: Yan Sui,

https://doi.org/10.1021/acs.macromol.5c00595
Macromolecules 2025, 58, 6883−6896

Zixiao Yang, Yichun Zhao, Xiaoyu Kong, and Dongluo Wu. Investigation and analysis: Yan Sui, Tingting Yin, and Xian Kong. Writing—original draft: Yan Sui. Writing—review-editing: Yan Sui and Xian Kong. Funding acquisition: Xian Kong.

Notes

The authors declare no competing financial interest.

■ ACKNOWLEDGMENTS

This research has been supported by the Major Research Plan of the National Natural Science Foundation of China (No. 92372104), the Guangdong Science and Technology Department (No. 2023QN10C439), the Guangdong Basic and Applied Basic Research Foundation (No. 2022A1515110016 and 2024B1515040023), the Guangzhou Municipal Science and Technology Bureau (No. 2023A04J1364), the 111 Project (No. B18023), and the Fundamental Research Funds for the Central Universities (No. 2024ZYGXZR043). This work is partially supported by the High Performance Computing Platform of South China University of Technology.

■ REFERENCES

(1) Simon, P.; Gogotsi, Y. Materials for electrochemical capacitors. *Nat. Mater.* **2008**, *7*, 845−854.
(2) Gogotsi, Y.; Simon, P. True performance metrics in electrochemical energy storage. *Science* **2011**, *334*, 917−918.
(3) Zhang, S.; Pan, N. Supercapacitors performance evaluation. *Adv. Energy Mater.* **2015**, *5*, 1401401.
(4) Wang, Y.; Song, Y.; Xia, Y. Electrochemical capacitors: mechanism, materials, systems, characterization and applications. *Chem. Soc. Rev.* **2016**, *45*, 5925−5950.
(5) Simon, P.; Gogotsi, Y. Charge storage mechanism in nanoporous carbons and its consequence for electrical double layer capacitors. *Philos. Trans. R. Soc., A* **2010**, *368*, 3457−3467.
(6) Lewandowski, A.; Galinski, M. Practical and theoretical limits for electrochemical double-layer capacitors. *J. Power Sources* **2007**, *173*, 822−828.
(7) Tang, Z.; Tang, C.-h.; Gong, H. A High Energy Density Asymmetric Supercapacitor from Nano-architectured Ni(OH)2/Carbon Nanotube Electrodes. *Adv. Funct. Mater.* **2012**, *22*, 1272−1278.
(8) Hall, P. J.; Mirzaeian, M.; Fletcher, S. I.; Sillars, F. B.; Rennie, A. J.; Shitta-Bey, G. O.; Wilson, G.; Cruden, A.; Carter, R. Energy storage in electrochemical capacitors: designing functional materials to improve performance. *Energy Environ. Sci.* **2010**, *3*, 1238−1251.
(9) Fan, L.-Q.; Zhong, J.; Wu, J.-H.; Lin, J.-M.; Huang, Y.-F. Improving the energy density of quasi-solid-state electric double-layer capacitors by introducing redox additives into gel polymer electrolytes. *J. Mater. Chem. A* **2014**, *2*, 9011−9014.
(10) Simon, P.; Gogotsi, Y. Capacitive energy storage in nanostructured carbon−electrolyte systems. *Acc. Chem. Res.* **2013**, *46*, 1094−1103.
(11) Vatamanu, J.; Hu, Z.; Bedrov, D.; Perez, C.; Gogotsi, Y. Increasing energy storage in electrochemical capacitors with ionic liquid electrolytes and nanostructured carbon electrodes. *J. Phys. Chem. Lett.* **2013**, *4*, 2829−2837.
(12) Lian, C.; Liu, K.; Van Aken, K. L.; Gogotsi, Y.; Wesolowski, D. J.; Liu, H.; Jiang, D.; Wu, J. Enhancing the capacitive performance of electric double-layer capacitors with ionic liquid mixtures. *ACS Energy Lett.* **2016**, *1*, 21−26.
(13) Feng, G.; Li, S.; Presser, V.; Cummings, P. T. Molecular insights into carbon supercapacitors based on room-temperature ionic liquids. *J. Phys. Chem. Lett.* **2013**, *4*, 3367−3376.
(14) Bi, S.; Banda, H.; Chen, M.; Niu, L.; Chen, M.; Wu, T.; Wang, J.; Wang, R.; Feng, J.; Chen, T.; et al. Molecular understanding of charge storage and charging dynamics in supercapacitors with MOF electrodes and ionic liquid electrolytes. *Nat. Mater.* **2020**, *19*, 552−558.
(15) Feng, G.; Qiao, R.; Huang, J.; Dai, S.; Sumpter, B. G.; Meunier, V. The importance of ion size and electrode curvature on electrical double layers in ionic liquids. *Phys. Chem. Chem. Phys.* **2011**, *13*, 1152−1161.
(16) Yao, L.; Wu, Q.; Zhang, P.; Zhang, J.; Wang, D.; Li, Y.; Ren, X.; Mi, H.; Deng, L.; Zheng, Z. Scalable 2D hierarchical porous carbon nanosheets for flexible supercapacitors with ultrahigh energy density. *Adv. Mater.* **2018**, *30*, 1706054.
(17) Feng, L.; Wang, K.; Zhang, X.; Sun, X.; Li, C.; Ge, X.; Ma, Y. Flexible solid-state supercapacitors with enhanced performance from hierarchically graphene nanocomposite electrodes and ionic liquid incorporated gel polymer electrolyte. *Adv. Funct. Mater.* **2018**, *28*, 1704463.
(18) Kwon, D.-K.; Myoung, J.-M. Ion gel-based flexible electrochemiluminescence full-color display with improved sky-blue emission using a mixed-metal chelate system. *Chem. Eng. J.* **2020**, *379*, 122347.
(19) Feng, E.; Gao, W.; Yan, Z.; Li, J.; Li, Z.; Ma, X.; Ma, L.; Yang, Z. A multifunctional hydrogel polyelectrolyte based flexible and wearable supercapacitor. *J. Power Sources* **2020**, *479*, 229100.
(20) Kim, J.; Kim, J. W.; Kim, S.; Keum, K.; Park, J.; Jeong, Y. R.; Jin, S. W.; Ha, J. S. Stretchable, self-healable, and photodegradable supercapacitor based on a polyelectrolyte crosslinked via dynamic host-guest interaction. *Chem. Eng. J.* **2021**, *422*, 130121.
(21) Huang, Y.; Zhong, M.; Huang, Y.; Zhu, M.; Pei, Z.; Wang, Z.; Xue, Q.; Xie, X.; Zhi, C. A self-healable and highly stretchable supercapacitor based on a dual crosslinked polyelectrolyte. *Nat. Commun.* **2015**, *6*, 10310.
(22) Jin, X.; Sun, G.; Zhang, G.; Yang, H.; Xiao, Y.; Gao, J.; Zhang, Z.; Qu, L. A cross-linked polyacrylamide electrolyte with high ionic conductivity for compressible supercapacitors with wide temperature tolerance. *Nano Res.* **2019**, *12*, 1199−1206.
(23) Cho, K. G.; An, S.; Cho, D. H.; Kim, J. H.; Nam, J.; Kim, M.; Lee, K. H. Block copolymer-based supramolecular ionogels for accurate on-skin motion monitoring. *Adv. Funct. Mater.* **2021**, *31*, 2102386.
(24) Chao, H.; Wang, Z.-G. Effects of surface transition and adsorption on ionic liquid capacitors. *J. Phys. Chem. Lett.* **2020**, *11*, 1767−1772.
(25) Atkin, R.; Borisenko, N.; Drüschler, M.; Endres, F.; Hayes, R.; Huber, B.; Roling, B. Structure and dynamics of the interfacial layer between ionic liquids and electrode materials. *J. Mol. Liq.* **2014**, *192*, 44−54.
(26) Kondrat, S.; Feng, G.; Bresme, F.; Urbakh, M.; Kornyshev, A. A. Theory and simulations of ionic liquids in nanoconfinement. *Chem. Rev.* **2023**, *123*, 6668−6715.
(27) Demir, B.; Searles, D. J. Investigation of the ionic liquid graphene electric double layer in supercapacitors using constant potential simulations. *Nanomaterials* **2020**, *10*, 2181.
(28) Xu, K.; Shao, H.; Lin, Z.; Merlet, C.; Feng, G.; Zhu, J.; Simon, P. Computational insights into charge storage mechanisms of supercapacitors. *Energy Environ. Mater.* **2020**, *3*, 235−246.
(29) Tee, S. R.; Searles, D. J. Fully periodic, computationally efficient constant potential molecular dynamics simulations of ionic liquid supercapacitors. *J. Chem. Phys.* **2022**, *156*, 184101.
(30) Muthukumar, M. *Physics of Charged Macromolecules*; Cambridge University Press, 2023.
(31) Li, Z.; Wu, J. Density functional theory for polyelectrolytes near oppositely charged surfaces. *Phys. Rev. Lett.* **2006**, *96*, 048302.
(32) Wiegel, F. Adsorption of a macromolecule to a charged surface. *J. Phys. A: Math. Gen.* **1977**, *10*, 299.
(33) Linse, P. Adsorption of weakly charged polyelectrolytes at oppositely charged surfaces. *Macromolecules* **1996**, *29*, 326−336.
(34) Carrillo, J.-M. Y.; Dobrynin, A. V. Molecular dynamics simulations of polyelectrolyte adsorption. *Langmuir* **2007**, *23*, 2472−2482.

https://doi.org/10.1021/acs.macromol.5c00595
Macromolecules 2025, 58, 6883−6896

(35) Wang, L.; Liang, H.; Wu, J. Electrostatic origins of polyelectrolyte adsorption: Theory and Monte Carlo simulations. *J. Chem. Phys.* **2010**, *133*, 044906.
(36) Bagchi, D.; Nguyen, T. D.; Olvera de la Cruz, M. Surface polarization effects in confined polyelectrolyte solutions. *Proc. Natl. Acad. Sci. U.S.A.* **2020**, *117*, 19677−19684.
(37) Wang, R.; Ginzburg, V. V.; Jiang, J.; Wang, Z.-G. Adsorption of a polyelectrolyte chain at dielectric surfaces: effects of surface charge distribution and relative dielectric permittivity. *Macromolecules* **2023**, *56*, 7653−7662.
(38) Chang, Q.; Jiang, J. Adsorption of block-polyelectrolytes on an oppositely charged surface. *Macromolecules* **2021**, *54*, 4145−4153.
(39) Sethuraman, V.; McGovern, M.; Morse, D. C.; Dorfman, K. D. Influence of charge sequence on the adsorption of polyelectrolytes to oppositely-charged polyelectrolyte brushes. *Soft Matter* **2019**, *15*, 5431−5442.
(40) Sing, C. E.; Perry, S. L. Recent progress in the science of complex coacervation. *Soft Matter* **2020**, *16*, 2885−2914.
(41) Madinya, J. J.; Chang, L.-W.; Perry, S. L.; Sing, C. E. Sequence-dependent self-coacervation in high charge-density polyampholytes. *Mol. Syst. Des. Eng.* **2020**, *5*, 632−644.
(42) Chang, L.-W.; Lytle, T. K.; Radhakrishna, M.; Madinya, J. J.; Vélez, J.; Sing, C. E.; Perry, S. L. Sequence and entropy-based control of complex coacervates. *Nat. Commun.* **2017**, *8*, 1273.
(43) Rumyantsev, A. M.; Jackson, N. E.; Yu, B.; Ting, J. M.; Chen, W.; Tirrell, M. V.; De Pablo, J. J. Controlling complex coacervation via random polyelectrolyte sequences. *ACS Macro Lett.* **2019**, *8*, 1296−1302.
(44) Hastings, D. E.; Bozelli Jr, J. C.; Epand, R. M.; Stover, H. D. Investigating the Effects of Charge Arrangement in Stimuli-Responsive Polyelectrolytes. *Macromolecules* **2021**, *54*, 11427−11438.
(45) Lou, J.; Friedowitz, S.; Qin, J.; Xia, Y. Tunable Coacervation of Well-Defined Homologous Polyanions and Polycations by Local Polarity. *ACS Cent. Sci.* **2019**, *5*, 549−557.
(46) Friedowitz, S.; Lou, J.; Barker, K. P.; Will, K.; Xia, Y.; Qin, J. Looping-in complexation and ion partitioning in nonstoichiometric polyelectrolyte mixtures. *Sci. Adv.* **2021**, *7*, No. eabg8654.
(47) Jia, D.; Muthukumar, M. Dipole-driven interlude of mesomorphism in polyelectrolyte solutions. *Proc. Natl. Acad. Sci. U.S.A.* **2022**, *119*, No. e2204163119.
(48) Lee, C.-L.; Muthukumar, M. Phase behavior of polyelectrolyte solutions with salt. *J. Chem. Phys.* **2009**, *130*, 024904.
(49) Li, S.; Zhu, M.; Feng, G. The effects of dication symmetry on ionic liquid electrolytes in supercapacitors. *J. Phys.: Condens. Matter* **2016**, *28*, 464005.
(50) Kong, X.; Lu, D.; Liu, Z.; Wu, J. Molecular dynamics for the charging behavior of nanostructured electric double layer capacitors containing room temperature ionic liquids. *Nano Res.* **2015**, *8*, 931−940.
(51) Ahrens-Iwers, L. J. V.; Janssen, M.; Tee, S. R.; Meißner, R. H. ELECTRODE: An electrochemistry package for atomistic simulations. *J. Chem. Phys.* **2022**, *157*, 084801.
(52) Zeng, L.; Wu, T.; Ye, T.; Mo, T.; Qiao, R.; Feng, G. Modeling galvanostatic charge−discharge of nanoporous supercapacitors. *Nat. Comput. Sci.* **2021**, *1*, 725−731.
(53) Wang, Z.; Yang, Y.; Olmsted, D. L.; Asta, M.; Laird, B. B. Evaluation of the constant potential method in simulating electric double-layer capacitors. *J. Chem. Phys.* **2014**, *141*, 184102.
(54) Merlet, C.; Péan, C.; Rotenberg, B.; Madden, P. A.; Simon, P.; Salanne, M. Simulating supercapacitors: Can we model electrodes as constant charge surfaces? *J. Phys. Chem. Lett.* **2013**, *4*, 264−268.
(55) Reed, S. K.; Lanning, O. J.; Madden, P. A. Electrochemical interface between an ionic liquid and a model metallic electrode. *J. Chem. Phys.* **2007**, *126*, 084704.
(56) Siepmann, J. I.; Sprik, M. Influence of surface topology and electrostatic potential on water/electrode systems. *J. Chem. Phys.* **1995**, *102*, 511−524.
(57) Feng, G.; Cummings, P. T. Supercapacitor capacitance exhibits oscillatory behavior as a function of nanopore size. *J. Phys. Chem. Lett.* **2011**, *2*, 2859−2864.
(58) Yang, L.; Fishbine, B. H.; Migliori, A.; Pratt, L. R. Molecular simulation of electric double-layer capacitors based on carbon nanotube forests. *J. Am. Chem. Soc.* **2009**, *131*, 12373−12376.
(59) Santos, E.; Schmickler, W. On the timescale of electrochemical processes. *Electrochim. Acta* **2024**, *498*, 144659.
(60) Vatamanu, J.; Borodin, O.; Smith, G. D. Molecular Simulations of the Electric Double Layer Structure, Differential Capacitance, and Charging Kinetics for N-Methyl-N-propylpyrrolidinium Bis-(fluorosulfonyl)imide at Graphite Electrodes. *J. Phys. Chem. B* **2011**, *115*, 3073−3084.
(61) Sitlapersad, R. S.; Thornton, A. R.; den Otter, W. K. A simple efficient algorithm for molecular simulations of constant potential electrodes. *J. Chem. Phys.* **2024**, *160*, 034107.
(62) Limmer, D. T.; Merlet, C.; Salanne, M.; Chandler, D.; Madden, P. A.; Van Roij, R.; Rotenberg, B. Charge fluctuations in nanoscale capacitors. *Phys. Rev. Lett.* **2013**, *111*, 106102.
(63) Coskun, O. K.; Muñoz, M.; Dongare, S.; Dean, W.; Gurkan, B. E. Understanding the Electrode−Electrolyte Interfaces of Ionic Liquids and Deep Eutectic Solvents. *Langmuir* **2024**, *40*, 3283−3300.
(64) Kornyshev, A. A. Double-layer in ionic liquids: paradigm change? *J. Phys. Chem. B* **2007**, *111*, 5545−5557.
(65) Kohlrausch, R. Theorie des elektrischen Rückstandes in der Leidener Flasche. *Ann. Phys.* **1854**, *167*, 179−214.
(66) Cook, M.; Watts, D.; Williams, G. Correlation function approach to the dielectric behaviour of amorphous polymers. *Trans. Faraday Soc.* **1970**, *66*, 2503−2511.
(67) Williams, G.; Watts, D. C. Non-symmetrical dielectric relaxation behaviour arising from a simple empirical decay function. *Trans. Faraday Soc.* **1970**, *66*, 80−85.
(68) Wang, Z.; Chen, J.; Li, Y.; Dong, K.; Yu, Y. EDL structure of ionic liquid-MXene-based supercapacitor and hydrogen bond role on the interface: a molecular dynamics simulation investigation. *Phys. Chem. Chem. Phys.* **2022**, *24*, 5903−5913.
(69) Jiang, D.-e.; Jin, Z.; Henderson, D.; Wu, J. Solvent effect on the pore-size dependence of an organic electrolyte supercapacitor. *J. Phys. Chem. Lett.* **2012**, *3*, 1727−1731.
(70) Wu, J. Understanding the electric double-layer structure, capacitance, and charging dynamics. *Chem. Rev.* **2022**, *122*, 10821−10859.
(71) Goodwin, Z. A.; Kornyshev, A. A. Underscreening, overscreening and double-layer capacitance. *Electrochem. Commun.* **2017**, *82*, 129−133.
(72) Bazant, M. Z.; Storey, B. D.; Kornyshev, A. A. Double layer in ionic liquids: Overscreening versus crowding. *Phys. Rev. Lett.* **2011**, *106*, 046102.
(73) Kjellander, R. A multiple decay-length extension of the Debye−Hückel theory: to achieve high accuracy also for concentrated solutions and explain under-screening in dilute symmetric electrolytes. *Phys. Chem. Chem. Phys.* **2020**, *22*, 23952−23985.
(74) Bitsanis, I.; Hadziioannou, G. Molecular dynamics simulations of the structure and dynamics of confined polymer melts. *J. Chem. Phys.* **1990**, *92*, 3827−3847.
(75) Chatterjee, S.; Ganesh, P. S.; Chakraborty, M. Molecular insight into sequence-defined polyelectrolytes for energy storage devices. *Electrochim. Acta* **2024**, *491*, 144306.
(76) Dobrynin, A. V.; Rubinstein, M.; Joanny, J.-F. Adsorption of a polyampholyte chain on a charged surface. *Macromolecules* **1997**, *30*, 4332−4341.
(77) McNamara, J.; Kong, C.; Muthukumar, M. Monte Carlo studies of adsorption of a sequenced polyelectrolyte to patterned surfaces. *J. Chem. Phys.* **2002**, *117*, 5354−5360.
(78) Scalfi, L.; Salanne, M.; Rotenberg, B. Molecular Simulation of Electrode-Solution Interfaces. *Annu. Rev. Phys. Chem.* **2021**, *72*, 189−212.

https://doi.org/10.1021/acs.macromol.5c00595
Macromolecules 2025, 58, 6883−6896

(79) Plimpton, S.; Crozier, P.; Thompson, A. *LAMMPS-Large-Scale Atomic/Molecular Massively Parallel Simulator*; Sandia National Laboratories, 2007.
(80) Plimpton, S. Fast parallel algorithms for short-range molecular dynamics. *J. Comput. Phys.* **1995**, *117*, 1−19.
(81) Thompson, A. P.; Aktulga, H. M.; Berger, R.; Bolintineanu, D. S.; Brown, W. M.; Crozier, P. S.; In't Veld, P. J.; Kohlmeyer, A.; Moore, S. G.; Nguyen, T. D.; et al. LAMMPS-a flexible simulation tool for particle-based materials modeling at the atomic, meso, and continuum scales. *Comput. Phys. Commun.* **2022**, *271*, 108171.

https://doi.org/10.1021/acs.macromol.5c00595
Macromolecules 2025, 58, 6883−6896

Supporting Information for

Tunable Electric Double-Layer Capacitor Performance through Engineered Charge Patterns in Polyelectrolytes.

Yan Sui [1], Tingting Yin [1], Zixiao Yang [1], Yichun Zhao [1], Xiaoyu Kong [1], Dongluo Wu [1], Jiajia Zhou [1, 2], Xiupeng Chen [1], Xian Kong [1,2] *

[1] South China Advanced Institute for Soft Matter Science and Technology, School of Emergent Soft Matter, South China University of Technology, Guangzhou 510640, China
[2] Guangdong Provincial Key Laboratory of Functional and Intelligent Hybrid Materials and Devices, South China University of Technology, Guangzhou 510640, China

Xian Kong
Email: xk@scut.edu.cn

Simulation methods.

All our MD simulations were performed using the LAMMPS program[1-3]. In our coarse-grained molecular dynamics simulation, polyelectrolytes are represented by a linear bead-spring chain with a regular-patterned or block-patterned of charged beads. The number of charged beads on the polyelectrolyte chain is governed by the charge fraction f_q (the ratio of charged beads to the total number of beads, each charged beads carrying an electron charge of $-e$ or $+e$), and the bead diameter is 0.35 nm. The chain length of the polyelectrolyte is fixed at 20, We investigated five charge fractions (f_q = 0.1, 0.2, 0.3, 0.5 and 0.8). The polycationic and polyanionic chains have identical lengths and charge distributions. We used 170 polyanion chains (n_{PA} = 170) and polycation chains (n_{PC} = 170) to maintain charge neutrality. Each electrode was modeled as two layers of graphite, each containing 936 carbon atoms, oriented with the basal plane facing the electrolyte. The carbon atoms are hexagonally arranged in a zigzag configuration, with an interatomic spacing of 0.25 nm. The electrodes are modeled as ideal conductors, rendering the inclusion of a Thomas-Fermi screening length unnecessary. The solvent is a continuum background with uniform dielectric constant ε = 80. The simulation box dimensions were carried out in a $L_x \times L_y \times L_z$ rectangular cuboid box, where L_x =8.125 nm, L_y = 8 .22724 nm, L_z = 16 nm, and the effective z space was about 14.28 nm. Periodic boundary conditions are used in x and y directions and Weeks-Chandler-Andersen (WCA) terms are introduced to account for excluded volume interaction effects. The long-range Coulomb interaction is calculated by particle-particle particle-mesh (PPPM) with an accuracy of 10^{-7}. We integrate the equations of motion using a Verlet algorithm[4] in the canonical ensemble with Langevin thermostat using a reduced timestep of 2 fs. Starting from the initial configuration, the relaxation process took 10 ns, followed by another 20 ns to apply a potential difference, the first 2 ns to achieve equilibrium, and the subsequent time were used for data collection. All simulations are performed at a temperature T = 363 K.

The nonbonded interaction between the particles is modeled by the standard LJ potential with the cutoff distance of r_c = 0.39 nm. All atom pairs interact via an identical Lennard-Jones potential, characterized by a zero-crossing distance of 0.35 nm. All bonds are modeled as harmonic springs with the potential energy with equilibrium length of 0.39 nm.

We employ an improved constant potential method (CPM)[5] with a Gaussian parameter of η = 0.1979 nm^{-1}, representing the reciprocal width of the electrode charge smearing. This method enables a “doubled cell” simulation, where two capacitors are arranged back-to-back with opposite polarities to form a zero-dipole supercell (Figure S1).

To minimize artificial interactions between the two capacitors, a finite gap is introduced, ensuring that each capacitor operates independently and that their respective electrostatic environments remain unaffected by one another.

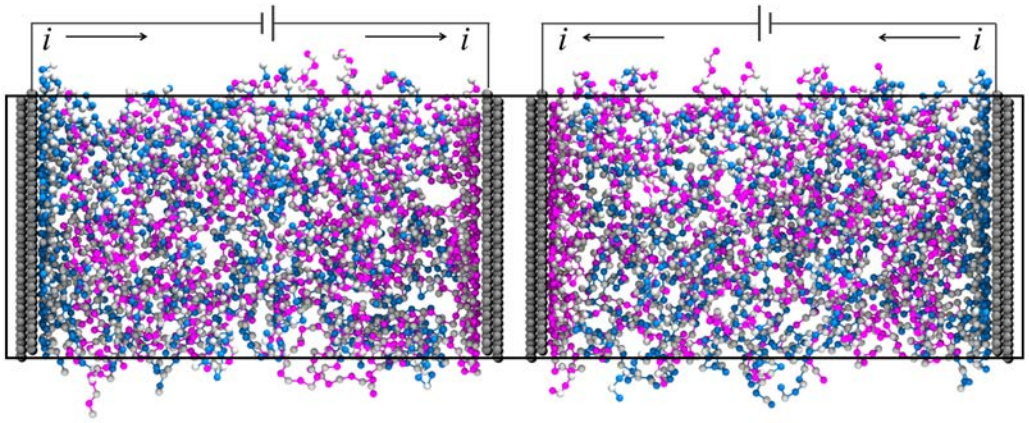

Figure S1. Electric double-layer capacitors (EDLC) with polyelectrolyte (PE) solution as working electrolytes. CPM method, which enables the concurrent execution of a “doubled cell” simulation, wherein two cells are arranged in a back-to-back configuration with opposite polarities to generate a zero-dipole super-cell. The bule beads represent polycation chains, the pink beads represent polyanion chains, and the gray beads represent carbon electrode atoms. The distance between the two planar electrodes is fixed at 14.28 nm. Black box is the PBC box.

Table S1 Summary of simulated systems

system	ρ_{total}	n_{PA}	n_{PC}	$N_{charged}$
f_q = 0.1	0.75	170	170	680
f_q = 0.2	0.75	170	170	1360
f_q = 0.3	0.75	170	170	2040
f_q = 0.5	0.75	170	170	3400
f_q = 0.8	0.75	170	170	5440

ρ is the overall bead number density.
n_{PA} is the number of polyanion chains.
n_{PC} is the number of polycation chains.
$N_{charged}$ is the total charged bead count.

Charge and electric potential rescaling.

The electrostatic potential Ψ due to a point charge q at a distance r in a medium with dielectric constant ε_r is given by $\Psi = \frac{1}{4\pi\varepsilon_0\varepsilon_r}\frac{q}{r}$. Rearranging this, we obtain $\Psi\sqrt{\varepsilon_r} = \frac{1}{4\pi\varepsilon_0}\frac{q/\sqrt{\varepsilon_r}}{r}$. Defining the rescaled potential $\Psi' = \Psi\sqrt{\varepsilon_r}$ and charge $q' = \frac{q}{\sqrt{\varepsilon_r}}$, we have $\Psi' = \frac{1}{4\pi\varepsilon_0}\frac{q'}{r}$, which corresponds to a system with vacuum dielectric constant. This scaling ensures that the electrostatic energy $U_{ele} = qV$ remains invariant, $U = q'\Psi' = \left(\frac{q}{\sqrt{\varepsilon}}\right)\left(\Psi\sqrt{\varepsilon}\right) = qV$. As can be verified, the Poisson equation follows similar effect after rescaling.

Energy storage performances.

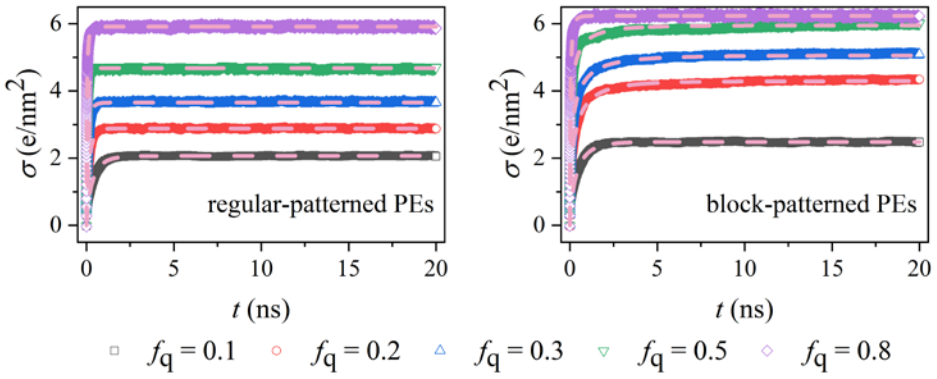

Figure S2. Time evolution of the charge density (σ) on the positive electrode of EDLC with working PEs of regular-patterned PEs and block-patterned PEs at a potential of 1 V. Pink dashed lines are KWW fitting curves based on Equation S2.

The exponential and KWW (Kohlrausch–Williams–Watts) fittings of the charging follows the following equations:

$$\sigma(t) = \sigma_{max}\left(1 - e^{-\frac{t}{RC}}\right) \quad \text{(S1)}$$

where σ_{max} is the equilibrium charge density, RC is the charging relaxation time constant.

$$\sigma(t) = \sigma_{max}\left(1 - e^{-\frac{t}{\tau}^{\beta}}\right) \quad \text{(S2)}$$

where τ is the charging relaxation time constant, and $\beta = 1/k_B T$ with k_B being the Boltzmann constant and T the temperature (363 K). β ($0 < \beta \leq 1$) is the stretching exponent that accounts for the distribution of relaxation times.

$$\tau_{avg} = \frac{\tau}{\beta} \cdot \Gamma\left(\frac{1}{\beta}\right) \quad \text{(S3)}$$

where Γ represents the Gamma function.

Table S2 The fitted parameters for regular-patterned PEs at 1 V

	Exponential function fitting			KWW fitting				
	σ_{max}	RC	R^2	σ_{max}	τ_{avg}	τ	β	R^2
f_q = 0.1	2.0636 ± 0.0002	0.3753 ± 0.0005	0.98	2.0670 ± 0.0001	0.3958 ± 0.0006	0.3497 ±0.0004	0.8011 ±0.0011	0.99
f_q = 0.2	2.8840 ± 0.0002	0.1627 ± 0.0002	0.98	2.8857 ± 0.0001	0.1701 ± 0.0002	0.1540 ±0.0002	0.8301 ±0.0011	0.99
f_q = 0.3	3.6486 ± 0.0002	0.0994 ± 0.0001	0.98	3.6504 ± 0.0001	0.1061 ± 0.0002	0.0929 ±0.0001	0.7906 ±0.0011	0.99
f_q = 0.5	4.6804 ± 0.0002	0.0562 ± 0.0001	0.97	4.6820 ± 0.0002	0.0611 ± 0.0001	0.0522 ±0.0001	0.7666 ±0.0014	0.98
f_q = 0.8	5.9110 ± 0.0003	0.0361 ± 0.0001	0.94	5.9135 ± 0.0002	0.0428 ± 0.0001	0.0326 ±0.0001	0.6756 ±0.0014	0.97

Table S3 The fitted parameters for block-patterned PEs at 1 V

	Exponential function fitting			KWW fitting				
	σ_{max}	RC	R^2	σ_{max}	τ_{avg}	τ	β	R^2
f_q = 0.1	2.4766 ± 0.0003	0.4489 ± 0.0007	0.97	2.4835 ± 0.0002	0.4852 ± 0.0008	0.4089 ±0.0005	0.7532 ±0.0011	0.99
f_q = 0.2	4.2468 ± 0.0009	0.3684 ± 0.0011	0.90	4.2929 ± 0.0004	0.5540 ± 0.0018	0.3103 ±0.0006	0.5338 ±0.0008	0.98
f_q = 0.3	4.9857 ± 0.0011	0.2623 ± 0.0010	0.83	5.0539 ± 0.0003	0.5087 ± 0.0015	0.2080 ±0.0004	0.4527 ±0.0005	0.99
f_q = 0.5	5.8999 ± 0.0010	0.1327 ± 0.0006	0.79	5.9551 ± 0.0006	0.3060 ± 0.0021	0.0969 ±0.0004	0.4076 ±0.0009	0.96
f_q = 0.8	6.2301 ± 0.0004	0.0469 ± 0.0001	0.93	6.2347 ± 0.0002	0.0592 ± 0.0002	0.0413 ±0.0001	0.6242 ±0.0011	0.98

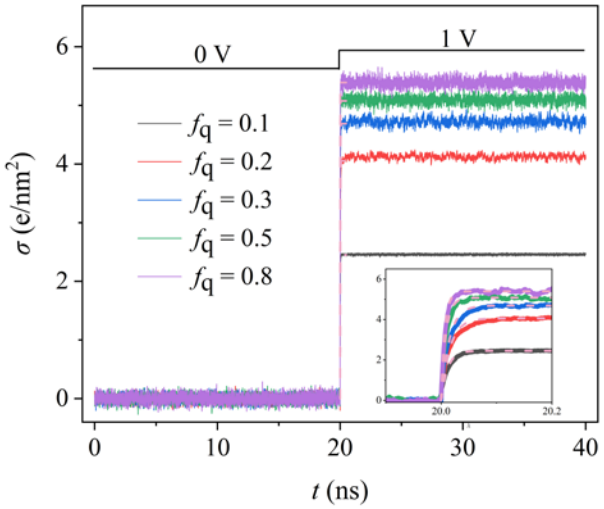

Figure S3. Time evolution of the charge density on the positive electrode of EDLC with working PEs of simple electrolyte. In the first 20 ns, the potential difference between two electrodes is 0 V. At 20 ns, the potential difference is set to 1 V. Pink dashed lines are exponential fitting curves. Insets magnify charge density near the positive electrode.

Table S4 The fitted parameters for simple electrolyte PEs at 1 V (Select the first 0.5 ns range)

	Exponential function fitting			KWW fitting				
	σ_{max}	RC	R^2	σ_{max}	τ_{avg}	τ	β	R^2
f_q = 0.1	2.4495 ± 0.0024	0.0115 ± 0.0002	0.95	2.4584 ± 0.0016	0.0128 ± 0.0002	0.0104 ±0.0001	0.7205 ±0.0083	0.98
f_q = 0.2	4.0548 ± 0.0050	0.0159 ± 0.0002	0.95	4.0908 ± 0.0022	0.0193 ± 0.0002	0.0143 ±0.0001	0.6572 ±0.0048	0.99
f_q = 0.3	4.6887 ± 0.0052	0.0147 ± 0.0002	0.96	4.7161 ± 0.0029	0.0168 ± 0.0002	0.0133 ±0.0001	0.6986 ±0.0063	0.99
f_q = 0.5	5.0764 ± 0.0041	0.0087 ± 0.0001	0.96	5.0875 ± 0.0032	0.0095 ± 0.0002	0.0080 ±0.0001	0.7607 ±0.0102	0.98
f_q = 0.8	5.3903 ± 0.0037	0.0067 ± 0.0001	0.97	5.3961 ± 0.0033	0.0071 ± 0.0001	0.0064 ±0.0001	0.8249 ±0.0126	0.98

Electric double layer structure.

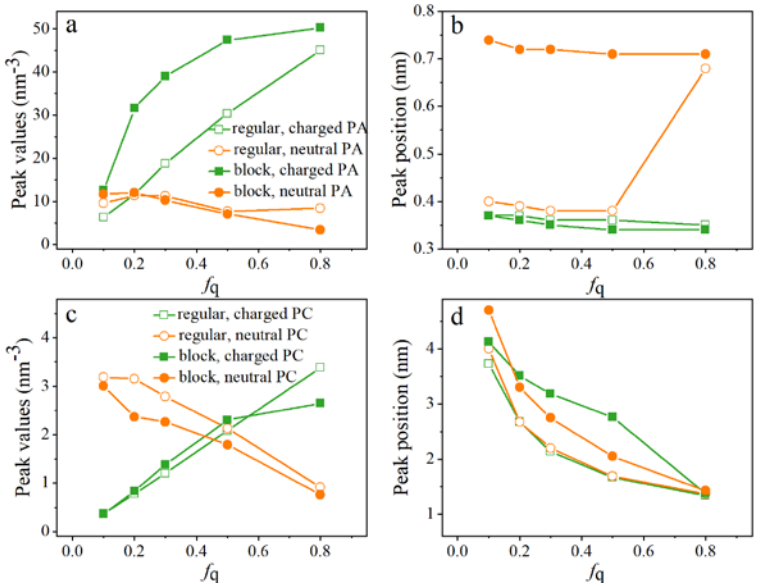

Figure S4. Quantitative comparison of EDLC structures based on the first peak in number density profiles. Peak values (a, c) and peak positions (b, d) of the first peak in number density profiles in Figure 3 (a) and (b) are for polyanion chains while (c) and (d) are for polycation chains.

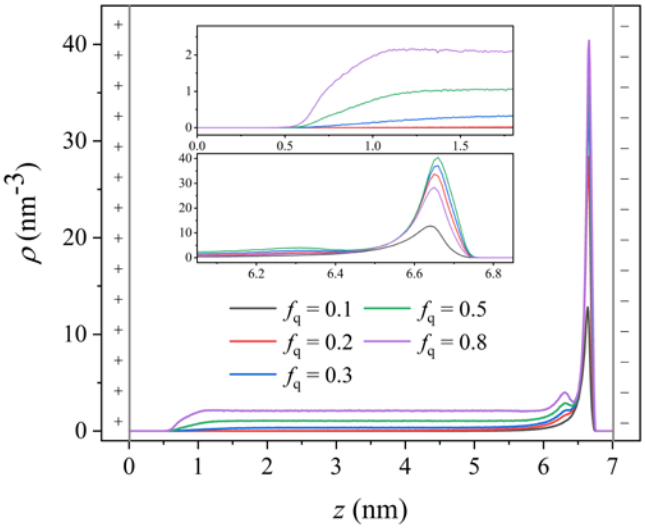

Figure S5. EDLC structure characterized by number density profile of different components along the normal direction of electrode surface for simple electrolyte. *z* is the distance from the outmost layer of atoms of positive electrode to the outmost layer of atoms of negative electrode. Insets magnify number density near the positive electrode and negative electrode, respectively.

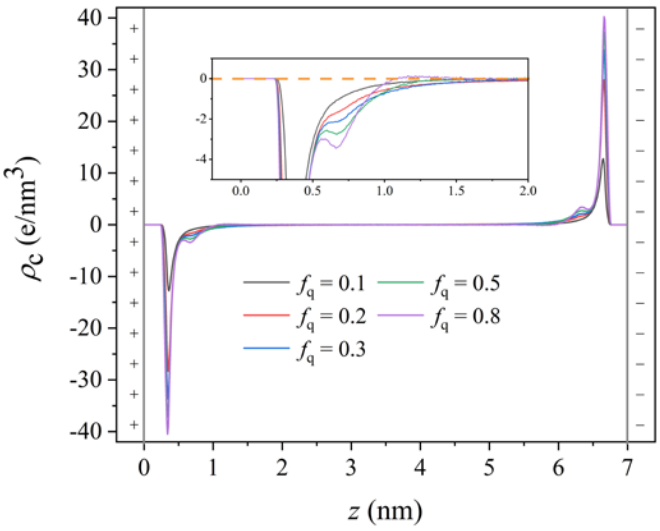

Figure S6. EDLC structure characterized by net charge density profile ρ_C (z) of different components along the normal direction of electrode surface for simple electrolyte. *z* is the distance from the outmost layer of atoms of positive electrode to the outmost layer of atoms of negative electrode. Insets magnify ρ_C (z) near the positive electrode.

PE adsorption dynamics.

The variation of adsorption counts of chain and charged beads over time can be described using the following exponential and KWW (Kohlrausch–Williams–Watts) functions:

$$\gamma = \gamma_{max} \cdot \left(1 - e^{\frac{t}{\tau}}\right) \tag{S4}$$

where γ_{max} is the equilibrium adsorption counts, τ is the relaxation time constant.

$$\gamma = \gamma_{max} \left(1 - e^{-\frac{t}{\tau}^{\beta}}\right) \tag{S5}$$

where $\beta = 1/k_B T$ with k_B being the Boltzmann constant and T the temperature (363 K), and β ($0 < \beta \leq 1$) is the stretching exponent that accounts for the distribution of relaxation times.

$$\tau_{avg} = \frac{\tau}{\beta} \cdot \Gamma\left(\frac{1}{\beta}\right) \tag{S6}$$

where Γ represents the Gamma function.

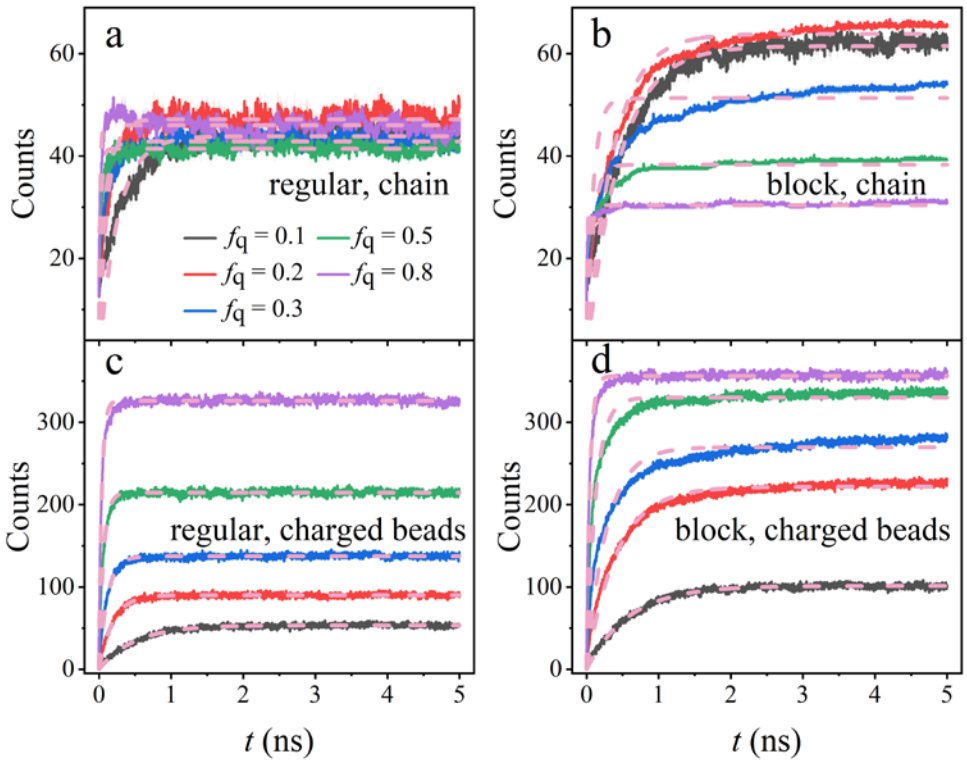

Figure S7. Time evolution of adsorption counts of polyelectrolyte chains (all beads) and charged bead at a potential of 1 V. Pink dashed lines are exponential fitting curves.

TableS5 The fitted parameters for adsorption counts of chain for regular-patterned PEs

	Exponential function fitting			KWW fitting				
	γ_{max}	τ	R^2	γ_{max}	τ_{avg}	τ	β	R^2
f_q = 0.1	43.8568 ± 0.0511	0.2594 ± 0.0026	0.84	45.0819 ± 0.0570	0.3746 ±0.0066	0.2239 ±0.0022	0.5563 ±0.0053	0.94
f_q = 0.2	47.1530 ± 0.0408	0.1145 ± 0.0013	0.80	47.4789 ± 0.0368	0.1396 ±0.0030	0.0941 ±0.0013	0.6064 ±0.0076	0.88
f_q = 0.3	42.8667 ± 0.0346	0.0693 ± 0.0009	0.70	43.2898 ± 0.0261	0.1104 ±0.0030	0.0511 ±0.0008	0.4803 ±0.0053	0.89
f_q = 0.5	41.4350 ± 0.0250	0.0253 ± 0.0004	0.63	41.5970 ± 0.0220	0.0423 ±0.0020	0.0183 ±0.0005	0.4645 ±0.0080	0.75
f_q = 0.8	45.9979 ± 0.0306	0.0141 ± 0.0004	0.46	46.0235 ± 0.0296	0.0158 ±0.0009	0.0114 ±0.0004	0.6410 ±0.0224	0.50

TableS6 The fitted parameters for adsorption counts of chain for block-patterned PEs

	Exponential function fitting			KWW fitting				
	γ_{max}	τ	R^2	γ_{max}	τ_{avg}	τ	β	R^2
f_q = 0.1	61.5058 ± 0.0578	0.4465 ± 0.0026	0.95	62.9149 ± 0.0616	0.5337 ± 0.0041	0.4283 ±0.0022	0.7118 ±0.0043	0.98
f_q = 0.2	63.8655 ± 0.0649	0.3626 ± 0.0026	0.92	66.3408 ± 0.0509	0.5283 ± 0.0038	0.3453 ±0.0015	0.5923 ±0.0026	0.99
f_q = 0.3	51.3398 ± 0.0680	0.2471 ± 0.0028	0.77	55.6758 ± 0.0610	0.7561 ± 0.0097	0.2439 ±0.0014	0.4105 ±0.0018	0.99
f_q = 0.5	38.2959 ± 0.0407	0.0834 ± 0.0014	0.52	39.8101 ± 0.0329	0.3058 ± 0.0089	0.0530 ±0.0006	0.3369 ±0.0024	0.96
f_q = 0.8	30.3754 ± 0.0156	0.0102 ± 0.0002	0.44	30.6777 ± 0.0131	0.0610 ± 0.0044	0.0050 ±0.0002	0.2830 ±0.0036	0.84

TableS7 The fitted parameters for adsorption counts of charged beads for regular-patterned PEs

	Exponential function fitting			KWW fitting				
	γ_{max}	τ	R^2	γ_{max}	τ_{avg}	τ	β	R^2
f_q = 0.1	53.5000 ± 0.0488	0.4880 ± 0.0026	0.97	53.6166 ±0.0546	0.4954 ±0.0033	0.4861 ±0.0027	0.9581 ±0.0076	0.97
f_q = 0.2	90.0042 ± 0.0448	0.1867 ± 0.0009	0.97	90.0872±0.0458	0.1897 ±0.0012	0.1842 ±0.0010	0.9384 ±0.0071	0.97
f_q = 0.3	137.2847±0.0521	0.1132 ± 0.0006	0.97	137.476 ±0.0501	0.1179 ±0.0008	0.1096 ±0.0006	0.8653 ±0.0060	0.97
f_q = 0.5	214.4908±0.0663	0.0617 ± 0.0003	0.96	214.738±0.0585	0.0657 ±0.0005	0.0584 ±0.0003	0.8076 ±0.0057	0.97
f_q = 0.8	325.9370±0.0906	0.0381 ± 0.0002	0.95	326.411 ±0.0689	0.0438 ±0.0004	0.0351 ±0.0002	0.7117 ±0.0048	0.97

TableS8 The fitted parameters for adsorption counts of charged beads for block-patterned PEs

	Exponential function fitting			KWW fitting				
	γ_{max}	τ	R^2	γ_{max}	τ_{avg}	τ	β	R^2
f_q = 0.1	101.3063±0.0665	0.5796 ± 0.0020	0.99	101.441±0.0759	0.5842 ± 0.0025	0.5789 ±0.0021	0.9794 ±0.0051	0.99
f_q = 0.2	221.6055±0.1361	0.4130 ± 0.0017	0.98	225.234 ±0.0945	0.4758 ± 0.0016	0.4061 ±0.0010	0.7651 ±0.0023	0.99
f_q = 0.3	269.6442±0.2566	0.2788 ± 0.0022	0.91	279.327 ±0.1570	0.4355 ± 0.0029	0.2699 ±0.0010	0.5701 ±0.0021	0.99
f_q = 0.5	329.9028±0.1984	0.1263 ± 0.0009	0.92	333.511 ±0.1050	0.1721 ± 0.0013	0.1147 ±0.0006	0.6015 ±0.0027	0.99
f_q = 0.8	356.1528±0.0990	0.0482 ± 0.0003	0.96	356.793±0.0693	0.0553 ± 0.0004	0.0448±0.0002	0.7196 ±0.0039	0.98

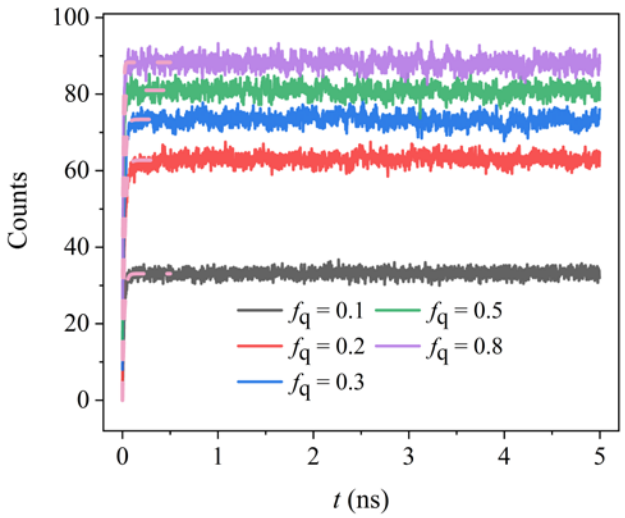

Figure S8. Time evolution of the adsorbed counts for simple electrolyte. Pink dashed lines are exponential fitting curves.

TableS9 The fitted parameters for adsorption counts of charged beads for simple electrolyte (Select the first 0.5 ns range)

	Exponential function fitting			KWW fitting				
	γ_{max}	τ	R^2	γ_{max}	τ_{avg}	τ	β	R^2
f_q = 0.1	32.3144 ± 0.0667	0.0184 ± 0.0004	0.95	32.2977 ± 0.0677	0.0183 ± 0.0007	0.0186 ±0.0004	1.0401 ±0.0342	0.95
f_q = 0.2	61.2328 ± 0.1044	0.0204 ± 0.0003	0.97	61.5016 ± 0.0959	0.0220 ± 0.0006	0.0196 ±0.0003	0.8087 ±0.0165	0.98
f_q = 0.3	72.3957 ± 0.1061	0.0174 ± 0.0003	0.97	72.6112 ± 0.0955	0.0184 ± 0.0005	0.0166 ±0.0003	0.8239 ±0.0159	0.98
f_q = 0.5	80.6977 ± 0.1326	0.0095 ± 0.0002	0.93	80.8906 ± 0.1225	0.0103 ± 0.0004	0.0088 ±0.0002	0.7636 ±0.0238	0.95
f_q = 0.8	87.9285 ± 0.1495	0.0065 ± 0.0002	0.89	88.1221 ± 0.1340	0.0073 ± 0.0004	0.0059 ±0.0002	0.7171 ±0.0291	0.91

SI References

1. Plimpton, Steve and Crozier, Paul and Thompson, Aidan, LAMMPS-large-scale atomic/molecular massively parallel simulator. *SNL*. 18, 43(2007).
2. Plimpton, Steve. Fast parallel algorithms for short-range molecular dynamics. *J. Comput. Phys*. 1117, 1-19(1995).
3. Thompson, A. et al. LAMMPS-a flexible simulation tool for particle-based materials modeling at the atomic, meso, and continuum scales. *Comput. Phys. Commun*. 271, 108171(2022).
4. Verlet, Loup. Computer" experiments" on classical fluids. I. Thermodynamical properties of Lennard-Jones molecules. *Phys. Rev*. 159, 9(1967).
5. Ahrens-Iwers, L. J. V.; Janssen, M.; Tee, S. R.; Meiβner, R. H. ELECTRODE: An electrochemistry package for atomistic simulations. *J. Chem. Phys*.157, 084801(2022).